

August 2013

## 3D Modeling and Design Optimization of Rod Shaped Ionic Polymer Metal Composite Actuator

Siul A. Ruiz

University of Nevada, Las Vegas, [Ruizs8@unlv.nevada.edu](mailto:Ruizs8@unlv.nevada.edu)

Follow this and additional works at: <https://digitalscholarship.unlv.edu/thesesdissertations>



Part of the [Engineering Science and Materials Commons](#), [Materials Science and Engineering Commons](#), [Mathematics Commons](#), and the [Mechanical Engineering Commons](#)

---

### Repository Citation

Ruiz, Siul A., "3D Modeling and Design Optimization of Rod Shaped Ionic Polymer Metal Composite Actuator" (2013). *UNLV Theses, Dissertations, Professional Papers, and Capstones*. 2829.  
<https://digitalscholarship.unlv.edu/thesesdissertations/2829>

This Thesis is protected by copyright and/or related rights. It has been brought to you by Digital Scholarship@UNLV with permission from the rights-holder(s). You are free to use this Thesis in any way that is permitted by the copyright and related rights legislation that applies to your use. For other uses you need to obtain permission from the rights-holder(s) directly, unless additional rights are indicated by a Creative Commons license in the record and/or on the work itself.

This Thesis has been accepted for inclusion in UNLV Theses, Dissertations, Professional Papers, and Capstones by an authorized administrator of Digital Scholarship@UNLV. For more information, please contact [digitalscholarship@unlv.edu](mailto:digitalscholarship@unlv.edu).

3D MODELING AND DESIGN OPTIMIZATION OF ROD SHAPED IONIC  
POLYMER METAL COMPOSITE ACTUATOR

By

Siul Ruiz

Bachelor of Science in Mechanical Engineering  
University of Nevada Las Vegas  
2011

Bachelor of Science in Mathematics  
University of Nevada Las Vegas  
2011

A thesis submitted in partial fulfillment  
of the requirements for the

Master of Science in Engineering - Mechanical Engineering

Department of Mechanical Engineering  
Howard R. Hughes College of Engineering  
The Graduate College

University of Nevada, Las Vegas  
August 2013



## THE GRADUATE COLLEGE

We recommend the thesis prepared under our supervision by

**Siul Ruiz**

entitled

**3D Modeling and Design Optimization of Rod Shaped Ionic Polymer Metal Composite Actuator**

be accepted in partial fulfillment of the requirements for the degree of

**Master of Science in Engineering – Mechanical Engineering**  
Department of Mechanical Engineering

Woosoon Yim, Ph.D., Committee Chair

Kwan Kim, Ph.D., Committee Member

Mohamed Tribia, Ph.D., Committee Member

Markus Berli, Ph.D., Graduate College Representative

Kathryn Hausbeck Korgan, Ph.D., Interim Dean of the Graduate College

**August 2013**

## ABSTRACT

### **3D Modeling And Design Optimization Of Rod Shaped Ionic Polymer-Metal Composite Actuator**

by

Siul Ruiz

Dr. Woosoon Yim, Examination Committee Chair  
Professor of Teaching and Learning  
University of Nevada, Las Vegas

Ionic polymer-metal composites (IPMCs) are some of the most well-known electro-active polymers. This is due to their large deformation provided a relatively low voltage source. IPMCs have been acknowledged as a potential candidate for biomedical applications such as cardiac catheters and surgical probes; however, there is still no existing mass manufacturing of IPMCs. This study intends to provide a theoretical framework which could be used to design practical purpose IPMCs depending on the end users interest.

This study begins by investigating methodologies used to develop quantify the physical actuation of an IPMC in 3-dimensional space. This approach is taken in two separate means; however, both approaches utilize the finite element method. The first approach utilizes the finite element method in order to describe the dynamic response of a segmented IPMC actuator. The first approach manually constructs each element with a local coordinate system. Each system undergoes a rigid body motion along the element and deformation of the element is expressed in the local coordinate frame. The physical phenomenon in this system is simplified by utilizing a lumped RC model in order to simplify the electro-mechanical phenomena in the IPMC dynamics.

The second study investigates 3D modeling of a rod shaped IPMC actuator by explicitly coupling electrostatics, transport phenomenon, and solid mechanics. This portion of the research will briefly discuss the mathematical background that more accurately quantifies the physical phenomena. Solving for the 3-dimensional actuation is explicitly carried out again by utilizing the finite element method. The numerical result is conducted in a software package known as COMSOL MULTIPHYSICS. This simulation allows for explicit geometric rendering as well as more explicit quantification of the physical quantities such as concentration, electric field, and deflection

The final study will conduct design optimization on the COMSOL simulation in order to provide conceptual motivation for future designs. Utilizing a multi-physics analysis approach on a three dimensional cylinder and tube type IPMC provides physically accurate results for time dependent end effector displacement given a voltage source. Simulations are conducted with the finite element method and are also validated with empirical evidences. Having an in-depth understanding of the physical coupling

provides optimal design parameters that cannot be altered from a standard electro-mechanical coupling. These parameters are altered in order to determine optimal designs for end-effector displacement, maximum force, and improved mobility with limited voltage magnitude. Design alterations are conducted on the electrode patterns in order to provide greater mobility, electrode size for efficient bending, and Nafion diameter for improved force. The results of this study will provide optimal design parameters of the IPMC for different applications.

## **ACKNOWLEDGEMENTS**

I would like to express my genuine appreciation to my advisor, Dr. Woosoon Yim. He has inadvertently become one of my greatest inspirations throughout my undergraduate and graduate years. Without his support and advice, none of this research would have been possible. Most importantly, without the courses that he taught, I would have had little incentive to pursue graduate studies within this field. In the same sense, I would also like to thank Dr. Kwang Kim. Since meeting Dr. Kim, I've learned many novel concepts pertaining to my current research endeavors. Kim also provided many of the specimens used in this research, as well as many of the methodologies. I would like to thank Dr. Mohamed B. Trabia for all of your help. Outside of help with coursework, Dr. Trabia was always willing to help answer questions to the best of his ability whether it was pertaining to topics never explicitly touched on in class, thoroughly critiquing grant proposals, and even basic life choices. I am especially grateful for all of his support. I would also like to express my most sincere gratitude to Dr. Markus Berli. Dr. Berli had helped me throughout my undergraduate career with research opportunities at the Desert Research Institute. Dr. Berli also assisted me over a summer as an advisor for an NSF-

REU grant that I obtained. His continual support leads me to even graduate studies. Through working with Dr. Berli, I have learned the fundamentals of becoming a researcher in engineering. Whether I was programming a dynamic autonomous load frame, to learning the finite element method, Dr. Berli was there to help answer any questions and concerns that I ever had throughout the process.

I would also like to thank Dr. Jagadeep Thota. Many of his courses played a crucial role in helping me to excel in my research. Dr. Thota was one of the most helpful people I have ever met, and his directions were always clear and straight forward. I appreciate everything that he has brought to this university. I would also like to thank Dr. Yitung Chen. Dr. Chen's courses have always been incredibly demanding, but the outcome is always so fulfilling. He has provided me with a robust theoretical backbone within the field of engineering. I would also like to acknowledge Dr. Brendan O'Toole. He has always been able to provide me with a letter of recommendation. I would like to also acknowledge Dr. Pushkin Kachroo. Dr. Kachroo re-ignited my passion for mathematics.

I would like to thank Benjamin Mead for all of his support and continuous hard work. Ben provided me with much of the experimental and empirical constants needed to conduct many of these theoretical studies. He has also been helpful in many of the courses we've taken together. I would like to acknowledge Eldon Goddard for much of his assistance with the details of the finite element method. I would also like to acknowledge Zach Mellinger for his support through graduate school.

I would like to acknowledge the National Science Foundation (Award No. 0958565) for their support for this project.



I would like to thank Joan Conway. Joan has been helping me with all of my academic endeavors for the past six years. If it was not for her tireless efforts, I would have never graduated. I would also like to acknowledge Christine Wallace. She helped me to support myself financially for my final semester of undergraduate studies. This gesture was very kind and unexpected, and I greatly appreciate this.

I would like to acknowledge my family and friends, specifically (in no particular order) Marlon Austria, Soraya Silverman, Francisco Sermano, Baldomero Corona, Mason McElroy, Eduardo Bañaga, Elliot Ploutz, Lizabeth Rodriguez, Antonio Montano, Oleg Bedderman, Ryan Sibert, Ross Ploutz, and Brock Engle. Without their continuous support, I would not be where I am in life.

I would like to thank my girlfriend Melanie Malfabon. Similar to Dr. Trabia, Melanie has been integral in many of the decisions I have made in the past two and a half years. She is one of the most level headed and genuine people I have ever met in my entire life.

Finally, I would like to acknowledge Dr. Dan Cook and Lillian Ratliff. These two people taught me not to fear ambition, but to embrace it. They taught me to do what I want to do and how I want to do it. They continuously inspire me every passing day. I appreciate their influence as well as their help.

## Table of Contents

Abstract.....	iii
Acknowledgements.....	vi
List of Tables .....	xi
List of Figures .....	xii
Chapter 1: Introduction.....	1
Literature Review.....	3
Research Objectives.....	8
Thesis Overview .....	8
Chapter 2: Electromechanical Methods .....	10
Ionic Polymer Metal Composite (IPMC) Actuators .....	10
Ionic Current Physics Based Model.....	11
Clumped RC Model .....	14
Summary.....	16
Chapter 3: Large Deflection Dynamic Model .....	18
Large Beam Deformation .....	18
Kinematic and Dynamic Analog from 2D to 3D Construction .....	19
Constructing the Dynamic Equations of Motion from the Energy Method.....	25
Simulation Results .....	28
Discussion.....	31
Chapter 4: 3D Multi-Physics Actuation Model .....	33
Ionic Model.....	33
Mechanics Model.....	36
Finite Element Implementation.....	40
Mesh-Optimization .....	44
End-Effector Displacement.....	52
Discussion.....	55
Chapter 5: Design Optimization .....	57
Optimization Implementation .....	57
Optimal Radius for End-Effector Displacement.....	61
Optimal Radius for Force Output .....	62
Optimal Voltage Configuration for Twisting .....	64
Discussion.....	68
Chapter 6: Conclusion.....	70

Appendix A: Greens Function solution for Linear partial differential equations .....	73
References .....	78
Curriculum Vitae .....	84

## LIST OF TABLES

Table 3.1 Values of constant expressions.....	28
Table 4.1 Values of constant expressions.....	35
Table 5.1 Initial values of parameter expressions.....	58
Table 5.2 Final Voltage Expressions in counter clockwork order.....	66

## LIST OF FIGURES

Figure 1.1 Actuation of a rod type IPMC[3].....	3
Figure 2.1: electro-mechanical model.....	12
Figure 2.2: Clumped R-C Model of an arbitrary element.....	15
Figure 3.1: Coordinate discretization for the finite element implementation.....	19
Figure 3.2: 1D Beam elements used to simulate IPMC deflection.....	20
Figure 3.3. Resistivity approximation.....	29
Figure 3.4. Deflection comparison.....	30
Figure 4.1. Initial IPMC Geometry a) isometric view b) cross-section view.....	41
Figure 4.2. Clamp boundaries a) Experimental b) Simulated.....	42
Figure 4.3. Cross sectional description of the boundaries.....	43
Figure 4.4. Finite element Normal Physics based mesh.....	45
Figure 4.5. Normal Physics based mesh near the clamp domain.....	46
Figure 4.6. User Defined Mesh with edge distribution.....	47
Figure 4.7. User Defined Mesh Extrusion.....	48
Figure 4.8. Clamp boundary comparison a) Default mesh, b) Manual mesh.....	49
Figure 4.9. Concentration comparison a) Default mesh, b) Manual mesh.....	50
Figure 4.10. Finite element mesh a) Triangular mesh b) Swept mesh.....	51
Figure 4.11. Concentration results for the design optimization mesh.....	52
Figure 4.12. Image of the end-effector displacement for the IPMC.....	53
Figure 4.12. Tip displacement vs time comparison.....	54
Figure 5.1. Parametrized construction of the electrode domains.....	59
Figure 5.2. Block diagram detailing dependent multi-physics phenomenon.....	60
Figure 5.3. Optimal radius for maximum tip displacement.....	62
Figure 5.4. Optimal radius for maximum Space Charge Density.....	63
Figure 5.5. IPMC with 8 electrode domains.....	65
Figure 5.6. Curl Displacement Optimization.....	66
Figure 5.7.Compression and expansion.....	67

## CHAPTER 1: INTRODUCTION

Ionic Polymer-metal composites (IPMCs) have been comprehensively analyzed in the recent decades due to their flexible characteristics as well as being light weight[2]. IPMCs are of special interest due to their low electric driving voltage, large deflection, and biocompatibility[2]. Due to these qualities, the materials have gained a significant amount of attention in the medical field, biomimetic, and micromechanic[1]. IPMC's are unique in that they operate in wet conditions making them ideal for underwater propulsion[1].

IPMCs generally consist of an ionic polymer material as an ion exchange membrane. These membranes are typically Nafion and Flemion[1]. The membrane is coated by a layer of a highly electrically conductive noble metal such as platinum or gold to make up the electrode domain. Within the ion exchange membrane, the anions are fixed to the polymer. When hydrated, cations become mobile in order to balance the overall charge of the material. When a potential difference is applied to the electrode coating, hydrated cations migrate due to the imposed electric field. The migration of cations drags the water along with them[1]. This causes pressure changes that result in swelling local to the cathode and contraction near the anode. This results in mechanical deflection.

Though IPMCs have become of interest to a variety of disciplines, there still exists a definitive gap between the theoretical modeling and practical purpose for IPMCs. This is in part due to simulation efforts being placed into modeling IPMCs as a finite dimensional state space dynamical system. This is accomplished through a direct coupling of a lumped RC-circuit with a state space dynamical model. Although this methodology suffices in designing closed loop controllers, it gives no further insight as to the possible implementations or improvements of IPMCs. Though there have been studies on manufacturing IPMCs in order to improve performance, there have been very few breakthroughs within the past decades in IPMC technology.

Recent studies show that it is possible to model the physics in depth through directly modeling each physical phenomenon coupled together. By coupling the electric field to the cation transport, the space charge density can be used to simulate the body force that bends the IPMC. This multi-physics approach also explicitly utilizes the full geometry of the IPMC within the simulation, thus providing in great detail the spatial effects and geometric parameters. This becomes of particular interest when studying a rod type IPMC in 3-dimensional space. Rod IPMCs have the ability to rotate about two axes when given four electrodes; however, due to their thickness, their bending magnitude is not as pronounced.

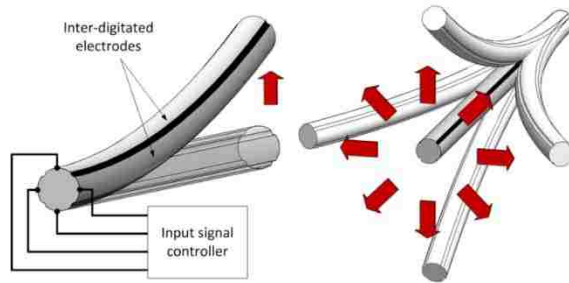


Figure 1.1 Actuation of a rod type IPMC[3]

## Literature Review

The conventional IPMC is a flat and very thin composite comprised of a thin ion-conductive polymer membrane with a thickness of up to  $100\mu\text{m}$ [7]. These membranes are typically constructed with a Nafion[1]. Membranes have been constructed with other polymers such as Flemion and Teflon[11]. Membranes are thinly coated with an electrode. These electrode coatings are typically noble metals with high electrical conductivity properties and low stiffness. Polymer membrane contains a fixed anion backbone as well as a solvent with mobile cations that balance the material charge. Usual cations used in an IPMC are  $\text{Li}^+$ ,  $\text{Na}^+$ ,  $\text{K}^+$ , and  $\text{Cs}^+$  in a water solution.

The design for an IPMC was first discovered by Shahinpoor *et al* in 1992[20,21]. This description lead to the design of swimming robotic structure based on IPMC actuation. One of the earliest works described the bending response of IPMCs saturated in water and bending in air. This study became more suitable for small deformations. This became a baseline for developing models amongst numerous researchers. The model used in [22] is based on a linear electromechanical coupling. This methodology utilized the similar



circuit models as that of piezoelectric elements. It was later proposed that the Young's modulus of an IPMC was transient, and thus, experiments were conducted to test this theory[23]. These procedures went in conjunction to viscoelastic models. Later modeling schemes made headway in quantifying non-uniform large deformations of IPMCs; however, these simulations failed to capture the transient behavior that truly describes the actuation[24]. Proposed distributed models describe the nonuniform bending of IPMCs by finding the curvature of any point along the IPMCs length [25]; however, these models fail to encompass the physical mechanical properties of the IPMC. A majority of the dynamic models above are limited to the bending of a single segment uniform IPMC.

The finite element models have become of particular interest in the fact that they are capable of dealing with non-linearity as well as discontinuities. Lee *et al* utilized commercial software to model an IPMC in a cantilever manner. The software was not capable of modeling the electromechanical coupling, thus a thermal analog was used to simulate the electromechanical coupling effects in the finite element model. A 2-dimensional finite element model was formulated based on the Galerkin method. Thus utilized the basic field equations governing the IPMC response by treating IPMCs as beams with two pairs of electrodes[25]. A 3-dimensional finite element model studied the deformation of IPMC beams based on the hydraulic distribution associated with the electrochemical response. Yim *et al*[4] made a first attempt to deal with this problem by utilizing a finite element modeling method to describe a segmented IPMC based on the large deflection beam theory. This work made use of a model that takes into account large deformations of the IPMC and uses this to describe the actuation. This model was limited in the fact that it could not accurately capture rigid body rotations of the elements.

Pugal *et al* [12, 17] used continuum mechanics equations in order to describe bending of the IPMC actuators. These models included mass transfer and electrostatic effects in the Nafion polymer; however, these models were restricted to small deformations in the case of IPMCs.

Many studies of IPMCs are primarily concerned with the electromechanical transduction phenomenon. The main distinguishing feature amongst many existing models is in the methodology of utilizing the necessary physics in order to describe this phenomenon. On one hand, studies are conducted utilizing empirical current-deflection relationship models. These models are frequently based on an electric circuit equivalent description used to quantify the effective effects of an electric field. On the other hand, other studies make attempts to explicitly model the ionic flux inside the polymer [1]. Both methods base the deflection on the electric currents; however, the explicit models calculate the charge directly in order to relate it to the body force or deflection while the circuit equivalent models make use of only the overall voltage or current to describe end-effector displacement or couple the current to the mechanical torque used to actuate a beam.

One effective circuit equivalent model was developed by Leo and Newbury. It was constructed in a manner such that all of the terms are frequency dependent and a viscoelastic model is explicitly utilized within the equations. The model allows for analysis of both actuation as well as sensing [27]. The grey box equivalent circuit model was introduced by Bonomo *et al.*, which were made up of two phases [28]. The first phase calculated the absorbed current provided an input voltage. The second phase estimated the blocking force or the tip displacement. Fractional order models were

developed by Cabonetto *et al.* by using Marquardt method for the least squares estimation[29]. Models were also developed in order to couple the applied voltage to the stress in the IPMC. These models also considered the effects of viscous fluids on the actuation performance of the material [30]. A three-stage model was developed by McDaid *et al.*. This consists of an equivalent circuit, electromechanical coupling term, and mechanical actuation stage [31]. This model was capable of describing an IPMCs actuation response given variable voltages up to 3V. This model also took into consideration the clamped section of the IPMC, thus making the simulation of the electric current precise. An open-end transmission line representation was proposed by Kruusmaa *et al.* in order to kinematically model an IPMC as a joint for a manipulator [32]. This work lead to the IPMCs being modeled as rigid elongation elements which can elongate rather than a long IPMC strip increases the controllability as well as the efficiency. A mathematically intensive derivation of a lossy circuit RC distributed line model was created to simulate an IPMC [25]. There do exist some models that use both electric circuits as well as physics based models. Branco and Dente use a continuum model of IPMC where a lumped-parametric circuit is derived to predict the relationship between applied voltage and current.

Purely physics based models explicitly consider the ionic current in the polymer and couple the computations directly to the solid mechanics of an IPMC. De Gennes first utilized a transport model for the ion and water molecules based on the systems entropy [33]. Nemat-Nasser proposed a broad theory of IPMC actuation [8], which he later proved two years later [34]. He utilized fundamental equations in order to describe the ionic flux, induced forces in Nafion, and the resulting IPMC deflection. Actuation models

based on electro-osmotic flow and pressure driven water flux were also developed at around this time by Asaka and Oguro[35].

Recent studies by Porfiri analyzed the charge dynamics and IPMC capacitance [36]. He proposed an analytic solution for the initial value problem based on matched asymptotic expansions. This analytic solution could then derive a circuit model for an IPMC. He also discussed how capacitance is a function of applied voltage. A similar approach was taken by Chen and Tan in order to develop a control design for IPMC. They solved the physics governed PDE based models in the Laplace domain and incorporated it in a control design by using model reduction [37]. Wallmersperger *et al.* demonstrated a large surface area effect on the electrode can be integrated into the ion transport model by augmenting the dielectric permittivity value and diffusion constant in respective equations [10]. This helps in that it avoids calculating highly nonlinear and very large cation concentrations in the electric potential gradients near the polymer boundaries. Akle *et al.* studied both computationally and empirically high surface area effects on induced current [38]. This study showed that higher electrode surface areas results in more stored charge and also different charge dynamics. Pugal conducted studies that utilized a multi-physics approach. This model used the boundary voltage conditions of the electrodes to drive the cation concentration. The space charge density driving the electric field in the polymer was a direct function of the cation concentration, thus the electric potential in the polymer changed with the cation concentration. He used these results to conduct a force coupling that drove the solid mechanical deflection.

## **Research Objectives**

This study takes advantage of the multi-physics simulation approach in order to conduct design optimizations that can be used to determine ideal rod type IPMC designs for different end users. There are four primary goals of this analysis. The first goal is to develop a mathematical description sufficient to effectively describe the physical phenomenon of a rod type IPMC in three dimensions. This will be implemented by coupling the physics describing the electric field, transport phenomenon, and the solid mechanics simultaneously. These equations will be solved for with the finite element method. The second goal is to produce a design that can maximize the end-effector displacement. By treating the rod diameter as a design parameter, optimization can be conducted in order to produce designs that maximize the end-effector displacement. The third goal is to provide a design that can be used to maximize the output force of an IPMC. This is done similarly by treating the rod diameter as a design parameter in order to maximize the volumetric body force output. The final goal of this study is to study small augmentations in the electrode pattern in order to determine a means to design an IPMC with the ability to twist. This final study conducts a basic parameterization on the electric potential boundary conditions in order to enable the rod type IPMC with the ability to rotate about its length.

## **Thesis Overview**

This thesis is organized as in a manner that details the IPMCs dynamic large deformation modeling, explicit multi-physical modeling with empirical evidence supporting the model, and design optimization in order to produce theoretical designs for a variety of end users.

Chapter 2 will provide a brief introduction to the underlying methods for IPMC actuation. This will touch on the two different types of electromechanical coupling methods typically used which include the circuit equivalent model and the explicit physical model.

Chapter 3 will provide a first approach at finite element modeling of an IPMC actuator. This model will describe the electromechanical actuation by utilizing a lumped RC model. This initial model allows for the simulation of large deformation. This methodology has an advantage when it comes to the implementation of a closed loop controller; however, this modeling method is not easily augmented for design optimization.

Chapter 4 will provide a second a second approach at finite element modeling of an IMPC actuator. This approach will utilize the multi-physical modeling approach used to explicitly quantify the ionic transport, the electric field, and the mechanical deflection. The finite element computations are conducted using software known as COMSOL MULTIPHYSICS. These simulations will be validated with empirical evidence.

Chapter 5 will investigate the methodology and results of the design optimization study. This will demonstrate designs that could increase the effective deflection, transmitted force, and propose designs that could potentially produce enhanced mobility.

## **CHAPTER 2: ELECTROMECHANICAL METHODS**

This chapter will first introduce the basic characteristics of IPMCs. The chapter will then present the two leading schools of thought in regards electromechanical coupling. The first that will be described is the explicit physics based methodology which utilizes fundamental first principles to describe the cation transport through the polymer domain. Based on the fundamental equations, the cation transport will drive the electric field within the polymer as well. The second will define an RC representation of the IPMC that is used to effectively define the electric field that drives the mechanical deflection.

### **Ionic Polymer Metal Composite (IPMC) Actuators**

The ionic polymer metal composite (IPMC) is a classification of electro active polymer (EAP). IPMCs are constructed from a base ionic polymer with an electrode coating. The material bends when subjected to a voltage across the thickness. IPMC have many desirable EAP characteristics. First of which is its driving voltage. With relatively low voltages of 1.0-5.0V, IPMCs exhibit large deflections. Second, IPMCs are relatively soft materials with a typical Young's modulus of  $E = 2.2 \times 10^8 Pa$ . In principle, IPMCs can be miniaturized to sizes under a millimeter. Lastly, IPMCs can be activated in water or in wet conditions. In fact, due to their need to be saturated, they work best in wet conditions.

IPMCs are also constructed from biocompatible materials. This combination of attributes makes IPMCs very attractive as an artificial muscle for biomimetics, biomechanics, or even biomedical applications. The IPMC used in this study is composed of a fluorinated ion exchange membrane (IEM) known as Nafion. This material is coated with a noble metal such as gold or platinum. These are used for their high conductivity and low stiffness.

When the polymer is hydrated, the cations become mobile. This allows the polymer to conduct cations. This ion mobility is proposed to be directly responsible for the electromechanical transduction in the ionic polymer transducer.

### **Ionic Current Physics Based Model**

The IPMC material consists of a polymer backbone with attached anion groups. The polymer is also saturated with a solvent that has mobile cations. When a voltage is applied to the electrodes of the IPMC, cation flux/ionic current is induced by the imposed electric field. In the case for water based IPMCs, cations drag the water molecules. This causes osmotic pressure changes. This induces swelling near the cathode and contraction near the anode. This can be explicitly seen as the deflection.



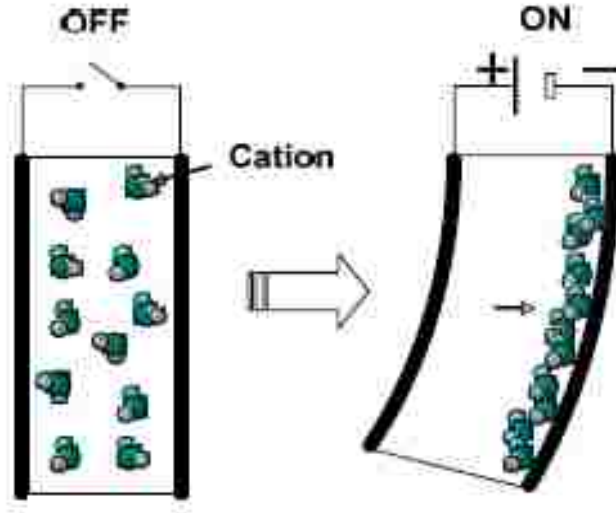


Figure 2.1: electro-mechanical model

This phenomenon is caused by an induced ionic current. This results in a non-zero space charge local to the electrode. The ionic current in the polymer is quantified by the Nernst-Plank Equation.

$$\frac{\partial c_c}{\partial t} - \nabla \cdot (D \nabla c_c + z\mu F c_c \nabla V_p + \mu c_c \Delta V P) = 0 \quad (2.1)$$

Where  $c_c$  is the cation concentration,  $\mu$  is the mobility of cations,  $D$  is the diffusivity constant,  $F$  is the Faraday constant,  $z$  is the charge number,  $\Delta V$  is the molar volume that quantifies the cation hydrophilicity,  $P$  is the solvent pressure, and  $V_p$  is the potential in the polymer. The mobility can be explicitly represented as

$$\mu = \frac{D}{RT} \quad (2.2)$$

where  $R$  is the gas constant and  $T$  is the absolute temperature. The Nernst-Plank equation is the primary governing equation that describes the ionic current through the polymer in

the IPMC. Aside from the transient term, the equation is composed of three different flux terms that are governed by different gradients:

- The electric potential gradient  $\nabla V_p$
- The concentration gradient  $\nabla c_c$
- The solvent pressure gradient  $\nabla P$

These field gradients are what drive the electromechanical model as well as the self-sensing mechanoelectrical model. For the interest of this study, this methodology will be used in order to properly evaluate the electromechanical model in chapter four.

This cation transport then becomes the driving term for the electric field in the polymer.

The potential  $V_p$  in the polymer domain is described by Poisson's equation:

$$-\nabla^2 V_p = \frac{\rho_s}{\epsilon} \quad (2.3)$$

where the  $\rho_s$  is the space charge and  $\epsilon$  is the dielectric permittivity. The space charge density is defined as

$$\rho_s = F(c_c - c_a) \quad (2.4)$$

where  $c_a$  is the anion concentration fixed to the backbone. The cation concentration is governed by the transport phenomena described by Nernst-Planck Equation; however, the anion concentration is related to local volumetric strain

$$\delta V = \nabla \cdot \mathbf{u} \quad (2.5)$$

where  $\mathbf{u}$  is the local displacement. This will be further elaborated in later chapters. The volume differences affect the anion concentration because the anions are what construct the polymer backbone. The anion concentration can be defined as

$$c_a = c_0(1 - \delta V) \quad (2.6)$$

where  $c_0$  is the initial anion/cation concentration.

The electric effects on the electrode domain are only briefly considered in this study. This is conducted with Ohms law

$$\mathbf{J} = -\sigma \nabla V_e \quad (2.7)$$

where  $\mathbf{J}$  is the current density in the electrodes,  $\sigma$  is the electric conductivity in the electrode, and  $V_e$  is the electric potential in the electrode. This potential interacts with the polymer potential; however, it is not the same variable as the polymer potential,  $V_p$ . This current conservation is briefly considered in the model; however, when considering mechanical design optimization, including this in the simulations became vastly too time consuming. An approximate method was considered and will later be explained in chapter 4.

### **Clumped RC Model**

The Clumped RC model relates the input voltage to the effective charge during actuation. For the cylindrical IPMCs, relaxation is not an issue, thus this will not be considered for this study. The design of an IPMC consists of parallel electrodes about a ionic conductor. These parallel electrodes act as a capacitor at the polymer-electrode interface. The polymer between electrodes are not as electrically conductive, thus the polymer is treated

as inducing a resistance. This C-R-C circuit can be simplified to an R-C circuit as shown in Figure 2.2 [4]

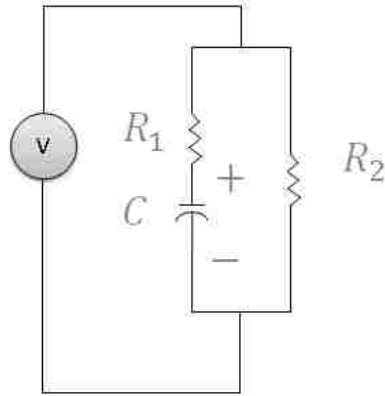


Figure 2.2: Clumped R-C Model of an arbitrary element

The relationship between voltage and charge can be expressed by the following equation

$$\frac{Q}{V} = \frac{C}{R_1 C s + 1} \quad (2.8)$$

where  $V$  is the voltage,  $Q$  is the electric charge,  $C$  is the capacitance. The direct relationship to electric current is represented as

$$\frac{I}{V} = \frac{C(R_1 + R_2)s + 1}{R_1 R_2 C s + R_2} \quad (2.9)$$

It should be noted that the equations are represented in the Laplace domain.

Under the influence of a voltage step input, the IPMC shows a deflection in the direction of the anode. This is due to the migration of cations directed towards the cathode within

the polymer matrix. The effective bending moment generated by the RC circuit is modeled by the following first order model

$$\frac{\mathbf{T}}{Q} = \frac{K_{\mathbf{T}}}{\tau_{\mathbf{T}}s+1} \quad (2.10)$$

where  $\mathbf{T}$  is the bending moment induced by the cation migration,  $K_{\mathbf{T}}$  is the gain,  $\tau_{\mathbf{T}}$  is the time constant.  $K_{\mathbf{T}}$  and  $\tau_{\mathbf{T}}$  characterize the speed and magnitude of the generated bending moment resulting from idealized charge moving across the thickness of the IPMC. By coupling these equations in the Laplace domain, the dynamic output can relate the input voltage  $V$  to the bending moment  $\mathbf{T}$ . This coupling can be seen as

$$\frac{\mathbf{T}}{V} = \frac{K_{\mathbf{T}}C}{\tau_Q\tau_{\mathbf{T}}s^2 + (\tau_Q + \tau_{\mathbf{T}})s + 1} \quad (2.11)$$

where  $\tau_Q = R_1C$ .

Based on [2], bi-axial bending could be produced by assuming two separate RC circuit models working in each direction. Though this is not completely accurate, this simplification suffices for most practical applications [39]

## Summary

This chapter investigated the two types of electromechanical coupling methodologies commonly used when studying IPMCs. The first method explicitly modeled the cation migration within the polymer domain through utilization of the Nernst-Planck partial differential equation to simulate the transport phenomena under the influence of an electric field. The electric field is produced as a combination of the boundary voltage condition as well as the change in the space charge density as the mobile cations migrate. The space charge density is the source term for the Poisson's equation that characterizes the

electric field within the polymer. This explicit method provides greater insight as to the underlying physics in play during the actuation of an IPMC; however, this methodology is more mathematically intensive.

The second methodology investigated is the lumped RC circuit methodology. This method utilizes a simplified characterization of the electric field by treating the IPMC as an RC circuit. This reduces the IPMC physical model down to a system of ordinary differential equations. The cation migration is implicitly quantified as the change in charge through the circuit. In the Laplace domain, this system can directly link the input voltage to the applied mechanical bending moment. Using two RC circuits, it is possible to approximate the dynamics of a biaxial IPMC actuator.

### **CHAPTER 3: LARGE DEFLECTION DYNAMIC MODEL**

This chapter will utilize a variation of large deflection beam bending theory in conjunction with the previously introduced lumped RC model in order to develop a dynamic model for IPMC actuation. First, the equations for large deflection for a beam will be introduced for a two dimensional model. These concepts will be used to produce a three dimensional large deflection beam model. This will lead to some theoretical results from the large beam deflection simulation. Finally, this chapter will discuss the advantages and disadvantages of this methodology of modeling.

#### **Large Beam Deformation**

From the results of Gutta and Yim[41], a dynamic model was developed for a flat IPMC undergoing large deformation. This model was implemented utilizing the finite element method. With this method, the 2D IPMC is segmented into individual beam elements which satisfy the Euler-Bernoulli theorem. An energy method was then used to construct the dynamic equations of motion. The applied bending moment is a result of the RC electrical model previously discussed in chapter 2.

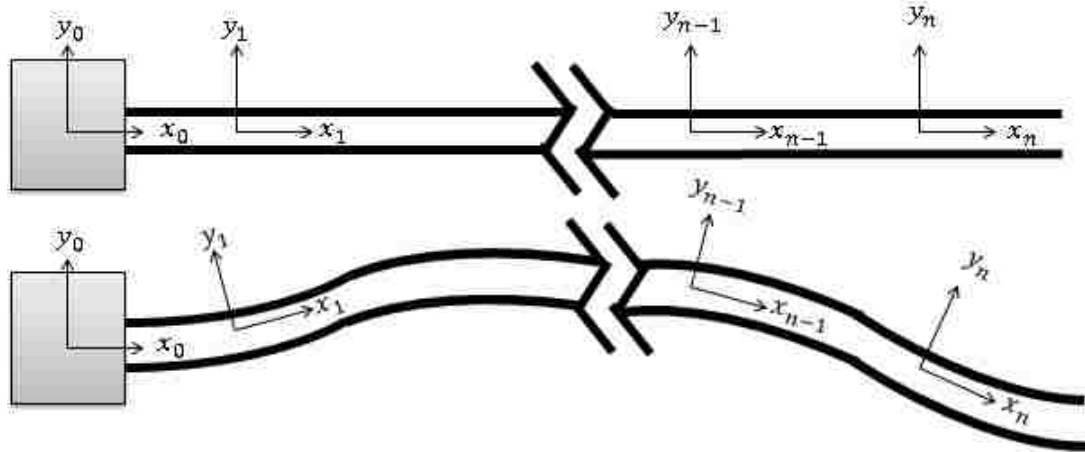


Figure 3.1: Coordinate discretization for the finite element implementation

The figure above illustrates a beam demonstrating the large deflection in a uniaxial bending IPMC. The beam is discretized into  $n$  segments. The inner white portion of the beam is constructed with the Ionomeric polymer Nafion. The thick black outer boundaries on the top and the bottom are constructed with a metallic electrode made of platinum. Ideally, the electrode could be selectively activated at each segment. Varying curvature along the length is obtained based on this assumption. By controlling the segmented IPMC, it gives the potential to use the actuator as a miniature robotic manipulator. In the following section, explicit modeling methodology will be discussed in order to construct the final model.

### **Kinematic and Dynamic Analog from 2D to 3D Construction**

This section conducts a study on the dynamics of the IPMC under the basis that it is comprised of  $n \in \mathbb{N}$  elements. An arbitrary element  $i \in \mathbb{N}$  lies between nodes  $i - 1$  and  $i$ . This element is defined by the local coordinate frame in, where node  $i - 1$  is locally



fixed. The orientation of the given  $i$ th frame has the same orientation of the slope at the stationary node  $i - 1$ . The displacement at an arbitrary point along the neutral axis of element  $i$  can be defined based on the local nodal displacements and the slopes of the nodes  $i - 1$  and  $i$ . To simplify the equations, the nodes  $i - 1$  and  $i$  will be labeled 1 and 2.

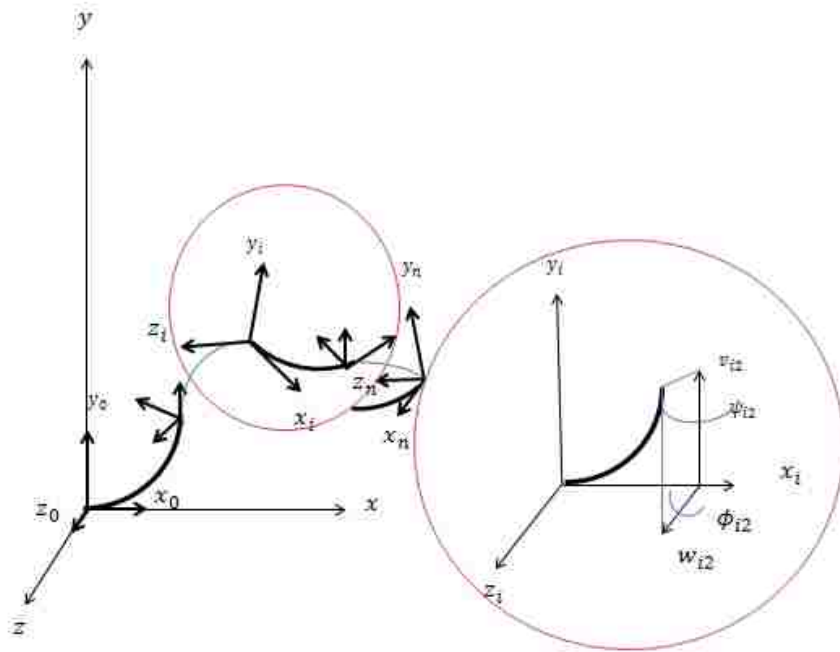


Figure 3.2: 1D Beam elements used to simulate IPMC deflection

For an element  $i$ , the displacement in the local  $y_i$  and the  $z_i$  directions can be described by the following equations:

$$v_i(x_i, t) = \mathbf{N}(x_i)q_{v,\phi,i}(t) \quad (3.1)$$

$$w_i(x_i, t) = \mathbf{N}(x_i)q_{w,\psi,i}(t) \quad (3.2)$$

Where

$$\mathbf{N}(x_i) = (N_1, N_2, N_3, N_4) \quad (3.3)$$

Is a row vector and

$$q_{v,\phi,i}(x_i, t) = (v_{i1}, \phi_{i1}, v_{i2}, \phi_{i2})^T \quad (3.4)$$

$$q_{w,\psi,i}(x_i, t) = (w_{i1}, \psi_{i1}, w_{i2}, \psi_{i2})^T \quad (3.5)$$

Are the column vectors such that  $v_{i1}, \phi_{i1}, w_{i1}$ , and  $\psi_{i1} = 0$ . These all denote the nodal displacements and the slopes in the first node of an arbitrary  $i$ th element. Likewise, that  $v_{i2}, \phi_{i2}, w_{i2}$ , and  $\psi_{i2}$  denote the displacement of the second node of an arbitrary  $i$ th element. The row vector  $\mathbf{N}(x_i)$  is composed of shape functions defined as follows[40]:

$$\begin{aligned} N_1 &= \frac{2x^2 - 3x^2L_i + L_i^3}{L_i^3} \\ N_2 &= \frac{x^3L_i - 2x^2L_i^2 + xL_i^3}{L_i^3} \\ N_3 &= \frac{-2x^3 + 3x^3L_i}{L_i^3} \\ N_4 &= \frac{x^3L_i + x^2L_i^2}{L_i^3} \end{aligned} \quad (3.6)$$

These vectors can be augmented in order to implement the equations in 3D space. This is done as follows:

$$q_i = (v_{i1}, \phi_{i1}, w_{i1}, \psi_{i1}, v_{i2}, \phi_{i2}, w_{i2}, \psi_{i2})^T \quad (3.7)$$

And the shape function vector becomes as follows:

$$\begin{aligned} \mathbf{N}_1(x_i) &= [N_1 \quad N_2 \quad 0 \quad 0 \quad N_3 \quad N_4 \quad 0 \quad 0] \\ \mathbf{N}_2(x_i) &= [0 \quad 0 \quad N_1 \quad N_2 \quad 0 \quad 0 \quad N_3 \quad N_4] \end{aligned} \quad (3.8)$$

The axial deformation is based on the lateral deformation of both directions. The differential form of the axial deformation can be expressed as follows:

$$du = -(ds - dx) \quad (3.9)$$

where  $dx$  is the infinitesimal axial deformation and  $ds$  is the length of a differential element which can be represented as follows:

$$ds = \sqrt{dv^2 + dw^2 + dx^2} \quad (3.10)$$

By substituting (3.9) into (3.8) and utilizing separation of variables, the following equation can be obtained:

$$\frac{du}{dx} = 1 - \sqrt{\left(\frac{dv}{dx}\right)^2 + \left(\frac{dw}{dx}\right)^2 + 1} \quad (3.11)$$

For a small enough magnitude,  $(l + 1)^p \approx pl + 1$ , thus (3.10) becomes

$$\frac{du}{dx} = -\frac{1}{2} \left( \left(\frac{dv}{dx}\right)^2 + \left(\frac{dw}{dx}\right)^2 \right) \quad (3.12)$$

And by integrating with respect to  $x$ , the following equation for axial deformation is produced:

$$u_i(x_i, t) = -\frac{1}{2} \int_0^{x_i} \left( \left( \frac{dv}{dx} \right)^2 + \left( \frac{dw}{dx} \right)^2 \right) dx$$

$$u_i(x_i, t) = q_i^T \left( -\frac{1}{2} \int_0^{x_i} (\mathbf{N}'_1(x)^T \mathbf{N}'_1(x) + \mathbf{N}'_2(x)^T \mathbf{N}'_2(x)) dx \right) q_i$$

$$u_i(x_i, t) = q_i^T (\mathbf{N}_s(x_i)) q_i \quad (3.13)$$

where  $\mathbf{N}'_1(x) = \frac{d\mathbf{N}_1(x)}{dx}$ ,  $\mathbf{N}'_2(x) = \frac{d\mathbf{N}_2(x)}{dx}$ , and  $\mathbf{N}_s(x_i) \in \mathbb{R}^{8 \times 8}$  is defined as

$$\mathbf{N}_s(x_i) = -\frac{1}{2} \int_0^{x_i} (\mathbf{N}'_1(x)^T \mathbf{N}'_1(x) + \mathbf{N}'_2(x)^T \mathbf{N}'_2(x)) dx \quad (3.14)$$

And so, the axial displacement of second node of a given element is given as

$$u_{i2}(t) = u_i(L_i, t) = q_i^T (\mathbf{N}_s(L_i)) q_i \quad (3.13)$$

With this, the global displacement vector can be defined by the following equation

$${}^i r_p = \sum_{j=1}^{i-1} \left( T_j \begin{pmatrix} L_j + q_j^T \mathbf{N}_s(L_j) q_j \\ \mathbf{N}_1(L_j) q_j \\ \mathbf{N}_2(L_j) q_j \end{pmatrix} \right) + T_i \begin{pmatrix} x_i + q_i^T \mathbf{N}_s(x_i) q_i \\ \mathbf{N}_1(x_i) q_i \\ \mathbf{N}_2(x_i) q_i \end{pmatrix} \quad (3.14)$$

where  $T_j \in \mathbb{R}^{2 \times 2}$  is the transformation matrix defined by the individual coordinate transformation matrices

$$T_j = T_{\Phi_j} T_{\Psi_j} \quad (3.15)$$

Where the  $T_{\Phi_j}$  and  $T_{\Psi_j} \in \mathbb{R}^{2 \times 2}$  are defined as

$$T_{\Phi_j} = \begin{pmatrix} \cos(\Phi_j) & -\sin(\Phi_j) & 0 \\ \sin(\Phi_j) & \cos(\Phi_j) & 0 \\ 0 & 0 & 1 \end{pmatrix} \quad (3.16)$$

and

$$T_{\Psi_j} = \begin{pmatrix} \cos(\Psi_j) & 0 & -\sin(\Psi_j) \\ 0 & 1 & 0 \\ \sin(\Psi_j) & 0 & \cos(\Psi_j) \end{pmatrix} \quad (3.17)$$

where  $\Psi_j$  and  $\Phi_j \in \mathbb{R}$  are defined as

$$\Phi_j = \sum_{k=1}^{j-1} \phi_{k2} \quad (3.18)$$

and

$$\Psi_j = \sum_{k=1}^{j-1} \psi_{k2} \quad (3.19)$$

where  $\phi_{k2}$  and  $\psi_{k2}$  represent the relative orientation of a given element  $k$ . It should also be noted that  $j \in \mathbb{N} \setminus \{1\}$ . With this formulation, the global velocity can be derived based on product rule as the following equation

$${}^i\dot{\gamma}_p = \sum_{j=1}^{i-1} \left( \dot{T}_j \begin{pmatrix} L_j + q_j^T \mathbf{N}_s(L_j) q_j \\ \mathbf{N}_1(L_j) q_j \\ \mathbf{N}_2(L_j) q_j \end{pmatrix} + T_j \begin{pmatrix} 2q_j^T \mathbf{N}_s(L_j) \dot{q}_j \\ \mathbf{N}_1(L_j) \dot{q}_j \\ \mathbf{N}_2(L_j) \dot{q}_j \end{pmatrix} \right) + \dot{T}_i \begin{pmatrix} x_i + q_i^T \mathbf{N}_s(x_i) q_i \\ \mathbf{N}_1(x_i) q_i \\ \mathbf{N}_2(x_i) q_i \end{pmatrix} + T_j \begin{pmatrix} 2q_j^T \mathbf{N}_s(x_i) \dot{q}_i \\ \mathbf{N}_1(x_i) \dot{q}_i \\ \mathbf{N}_2(x_i) \dot{q}_i \end{pmatrix} \quad (3.20)$$

where ,by product rule, the derivative of the transform can explicitly be expressed as

$$\dot{T}_j = \dot{T}_{\Phi_j} T_{\Psi_j} + T_{\Phi_j} \dot{T}_{\Psi_j} \quad (3.21)$$

Where, by chain rule

$$\dot{T}_{\Phi_j} = \sum_{k=1}^{j-1} \left( \frac{\partial T_{\Phi_j}}{\partial \phi_{k2}} \dot{\phi}_{k2} \right) \quad (3.21)$$

and

$$\dot{T}_{\Psi_j} = \sum_{k=1}^{j-1} \left( \frac{\partial T_{\Psi_j}}{\partial \psi_{k2}} \dot{\psi}_{k2} \right) \quad (3.22)$$

### Constructing the Dynamic Equations of Motion from the Energy Method

It is possible to represent equation (3.20) as the following

$${}^i \dot{r}_p = P_i \dot{\xi}_i \quad (3.23)$$

where

$$\xi_i = (v_{11}, \phi_{11}, w_{11}, \psi_{11}, v_{12}, \phi_{12}, w_{12}, \psi_{12} \dots, v_{i1}, \phi_{i1}, w_{i1}, \psi_{i1}, v_{i2}, \phi_{i2}, w_{i2}, \psi_{i2})$$

$$\xi_i = [q_1^T, q_2^T, \dots, q_{i-1}^T, q_i^T] \in \mathbb{R}^{8i} \quad (3.24)$$

represents the global coordinates in its entirety, and

$$P_i = \frac{\partial {}^i \dot{r}_p}{\partial \dot{\xi}_i} \in \mathbb{R}^{3 \times 8i} \quad (3.25)$$

represents the Jacobian that is to be multiplied by the global coordinates. With this representation, the equation for kinetic energy of a deformable body can be derived as

$$\begin{aligned} T_i &= \frac{\rho_i}{2} \int_0^{L_i} {}^i \dot{r}_p^T {}^i \dot{r}_p dx_i \\ &= \frac{\rho_i}{2} \dot{\xi}_i^T \left( \int_0^{L_i} P_i^T P_i dx_i \right) \dot{\xi}_i \\ &= \frac{1}{2} \dot{\xi}_i^T M_i \dot{\xi}_i \end{aligned} \quad (3.26)$$

where  $\rho_i$  is the elements density, and  $M_i$  is the mass matrix and can be described explicitly as

$$M_i = \rho_i \int_0^{x_i} P_i^T P_i dx \in \mathbb{R}^{8i \times 8i} \quad (3.27)$$

Similarly, the stiffness matrix can be derived in a similar manner. By analyzing the potential energy described by:

$$U_i = \frac{1}{2} \int_0^{L_i} \frac{1}{EI} \left( EI \left( \frac{\partial^2 v(x_i, t)}{\partial x_i^2} \right) + EI \left( \frac{\partial^2 w(x_i, t)}{\partial x_i^2} \right) + u_i \right)^2 dx \quad (3.28)$$

where  $v(x_i, t)$  and  $w(x_i, t)$  are the deflections at a given point on the  $i$ th element in the local frame,  $EI$  is the rotational rigidity based on the Young's elastic modulus and the area moment of inertia about the cross section of the IPMC. The stiffness matrix relies on the following

$$K_i = EI \int_0^{L_i} \left( \frac{\partial^2 \mathbf{N}_1(x_i)}{\partial x_i^2} \right)^T \left( \frac{\partial^2 \mathbf{N}_1(x_i)}{\partial x_i^2} \right) dx + EI \int_0^{L_i} \left( \frac{\partial^2 \mathbf{N}_2(x_i)}{\partial x_i^2} \right)^T \left( \frac{\partial^2 \mathbf{N}_2(x_i)}{\partial x_i^2} \right) dx \in \mathbb{R}^{8 \times 8} \quad (3.29)$$

where the stiffness is a function of the shape functions. In contrast to the mass matrix, the stiffness matrix only requires data from its local frame. Both need to be expanded to their entire length. These are represented by the following

$$M_{ei} = \begin{pmatrix} M_i & \mathbf{0}_{8n \times 8(n-i)} \\ \mathbf{0}_{8(n-i) \times 8n} & \mathbf{0}_{8(n-i) \times 8(n-i)} \end{pmatrix} \in \mathbb{R}^{8n \times 8n} \quad (3.30)$$

and

$$K_{ei} = \begin{pmatrix} \mathbf{0}_{8(i-1) \times 8(i-1)} & \mathbf{0}_{8(i-1) \times 8(i)} & \mathbf{0}_{8(i-1) \times 8(n-i)} \\ \mathbf{0}_{8(i) \times 8(i-1)} & K_i & \mathbf{0}_{8(i) \times 8(n-i)} \\ \mathbf{0}_{8(n-1) \times 8(n-1)} & \mathbf{0}_{8(n-1) \times 8(i)} & \mathbf{0}_{8(n-1) \times 8(n-i)} \end{pmatrix} \in \mathbb{R}^{8n \times 8n} \quad (3.31)$$

where  $\mathbf{0}_{j \times j}$  is a  $j \times j$  matrix of zeros. Based on the Lagrangian dynamic method, the equations of motion can be determined as follows

$$M_{ei}\ddot{\xi}_i + K_{ei}\xi_i = B_{ei}T_i(t), i \in \mathbb{N} \quad (3.32)$$

where

$$B_{ei} = \begin{pmatrix} \mathbf{0}_{8(i-1)} & \mathbf{0}_{8(i-1)} \\ 0 & 0 \\ 0 & 0 \\ 0 & 0 \\ 0 & 0 \\ 0 & 0 \\ 1 & 0 \\ 0 & 0 \\ 0 & 1 \\ \mathbf{0}_{8(n-i)} & \mathbf{0}_{8(n-i)} \end{pmatrix} \in \mathbb{R}^{8n \times 2} \quad (3.33)$$

is the control input used to apply the bending moment properly at the end of each element, and

$$T_i = \begin{pmatrix} T_{\psi_i} \\ T_{\phi_i} \end{pmatrix} \in \mathbb{R}^2 \quad (3.34)$$

defines the bending moment input that causes the deflection. This is directly related to the current as discussed in the chapter 2. Due to the initial node of a given element remains stationary within its relative inertial frame, it suffices to reduce the coordinates. This reduction is done by considering only the end-effector of a given element. This coordinate reduction explicitly becomes

$$\xi_e = (v_{12}, \phi_{12}, w_{12}, \psi_{12}, \dots, v_{n2}, \phi_{n2}, w_{n2}, \psi_{n2}) \in \mathbb{R}^{4n} \quad (3.35)$$

This then results in the reduction of the mass matrix,  $M_{ei} \in \mathbb{R}^{8n \times 8n} \Rightarrow M_{ei}^* \in \mathbb{R}^{4n \times 4n}$ , stiffness matrix,  $K_{ei} \in \mathbb{R}^{8n \times 8n} \Rightarrow K_{ei}^* \in \mathbb{R}^{4n \times 4n}$  and control input matrix,  $B_{ei} \in \mathbb{R}^{8n \times 2} \Rightarrow$



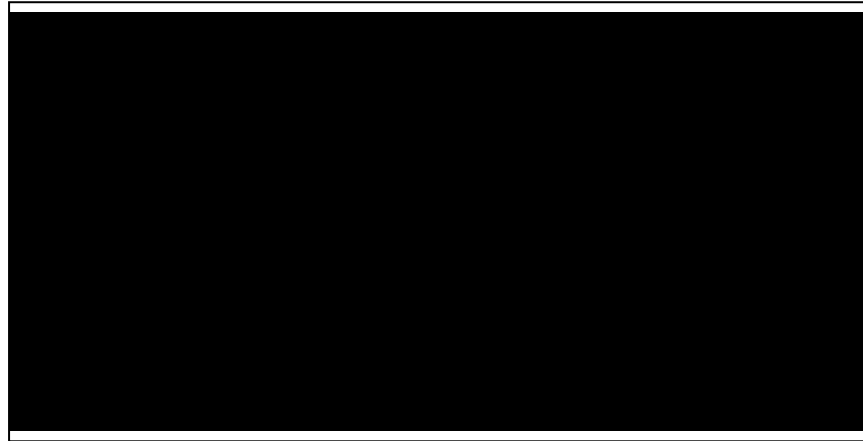
$B_{ei}^* \in \mathbb{R}^{4n \times 2}$ . Finally, the matrices are assembled producing a globally assembled mass matrix,  $M_e = \sum_{i=1}^n M_{ei}^* \in \mathbb{R}^{4n \times 4n}$ , stiffness matrix,  $K_e = \sum_{i=1}^n K_{ei}^* \in \mathbb{R}^{4n \times 4n}$ , the control input matrix,  $B_e = (B_{e1}^* \dots B_{en}^*) \in \mathbb{R}^{4n \times 2n}$ , and the input moment,  $T = (T_1 \dots T_n) \in \mathbb{R}^{2n}$ . This produces the final global dynamic equation of motion.

$$M_e \ddot{\xi}_e + K_e \xi_e = B_e T(t) \quad (3.36)$$

### Simulation Results

Establishing the physical parameters for the IPMC was the first step in order to run the simulation. The physical parameters are tabulated on table 3.1.

Table 3.1. Values of constant expressions.



Utilizing these values, a simulation for 3D deflection was constructed based on the large deflection theory provided in this chapter. The simulation was constructed in MATLAB

and SIMULINK. This model used a partitioned IPMC based on four elements. This model ran through a numerical solver which utilized two primary RC circuits at the base. Based on potential profile illustrated in an IPMC in [1], the applied voltage was manually reduced at the end of each element in order to approximate the effects of resistivity along the electrode length.

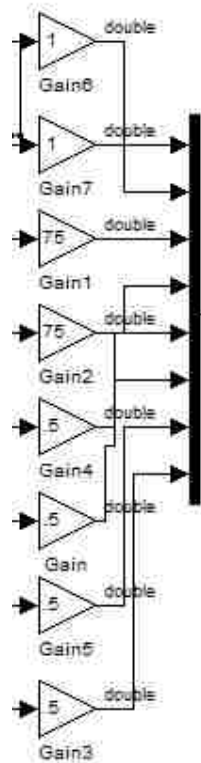


Figure 3.3. Resistivity approximation

The simulation end time was set for 5 seconds. The 3D simulation took over 36 hours to run. The end effector deflection was calculated based on the reduction in in length by the deflection in the y and z axis. The following plot was the result of the end effector

displacement of the simulation in comparison with the end effector displacement of the experiments.

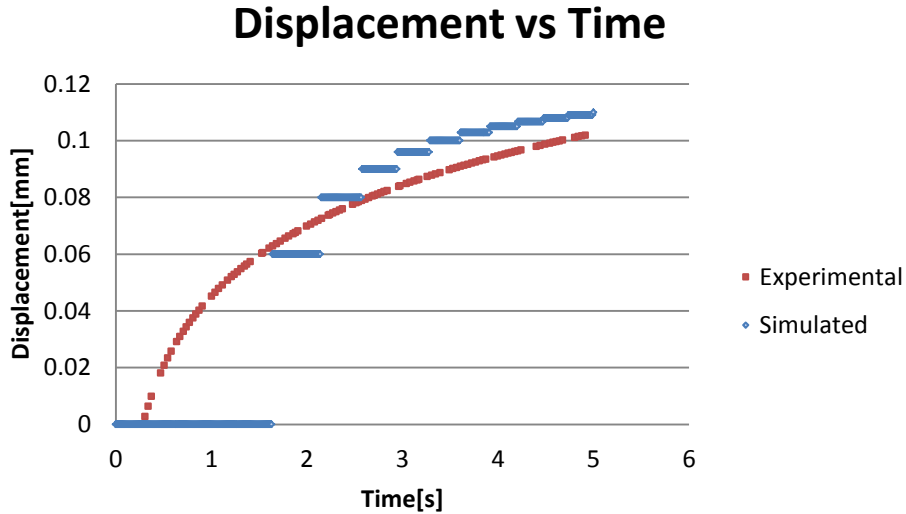


Figure 3.4. Deflection comparison

Based on the total end-effector deflection, it was possible to see a fairly close overall deflection between the two results. There appears to be a lag in the first second, but the result steps up pretty quickly thereafter. Some inaccuracies may be due to the time partitioning frequency. This could potentially be avoided by using a fixed step method for solving the system of ordinary differential equations. This simulation method provides some fairly accurate deflection results. This also seems to capture the dynamics of the system with a great deal of accuracy. The trend of both curves appears to converge at nearly the same rate as one another.

## **Discussion**

This methodology manages to capture many key features of IMPC actuation. With the ability to obtain the dynamics of the system in a frequency domain, it makes this model very attractive when applying feedback control laws to it. This methodology was much more computationally intensive than originally anticipated. It uses a tremendous amount of computational power. Simplification as well as optimization of this model could potentially be implemented in future work. As far as designing a feedback controller for the dynamic system, a model of this complexity is not entirely necessary. Based on the controller, the end effector will follow a fairly sophisticated response [39] with far less theoretical rigor.

This model fails to lend itself to design optimization. Because the simulation was conducted with rod type finite elements, the model does not hold geometric robustness. There is no novel way to predict optimal designs without manually reconstructing the model. Also, the RC circuit implementation also limits the ability to properly evaluate the geometric effects on the charge dynamics. The space-charge density from the explicit physics model relies heavily on the model's explicit geometry, and the space charge density governs the actuation process [1]. With this in mind, this model is not entirely ideal for conducting design optimization.

Lastly, due to the reduced magnitudes of deflection that come about from the rod type IPMC, a large deflection model is not necessarily needed in order to properly capture the actuation of the IPMC. This model does an excellent job when dealing with the flat type IPMC; however, the deflection magnitudes within a rod type IPMC can still be estimated with a great deal of accuracy with basic elastic isotropic mechanical principles.

Though this theory is a novel concept and could provide great insight on modeling methodologies in the future of feedback controllers, this method of study is far from ideal. In most every aspect of this study, it lacks the details necessary to properly be implemented. In contrast, this method becomes excessive in many areas which it could be more readily utilized. Though this methodology still holds a great deal of promise, it was not a proper fit for this study.

## **CHAPTER 4: 3D MULTI-PHYSICS ACTUATION MODEL**

This chapter will utilize a multi-physics approach to develop a 3D actuation model for the IPMC. The model will be developed in a software package known as COMSOL MULTIPHYSICS. This model will be designed with the explicit physics method previously tabulated. The implementation of the cation transport under the influence of an electric field in COMSOL will be demonstrated. This will be directly coupled with a standard linear elastic isotropic model in 3D space. In this mechanical section, a discussion will be made in regards to the force coupling methodology necessary for the future steps of the study. Furthermore, a brief discussion will be made in regards to mesh optimization necessary for physically accurate as well as timely results. Lastly, the actuation results from this model will be compared to the empirical actuation results. A brief discussion will be made in regards to potential inconsistencies as well as potential methods to make the model more accurate.

### **Ionic Model**

The following section defines the equations explicitly used in order to numerically solve the physical phenomenon

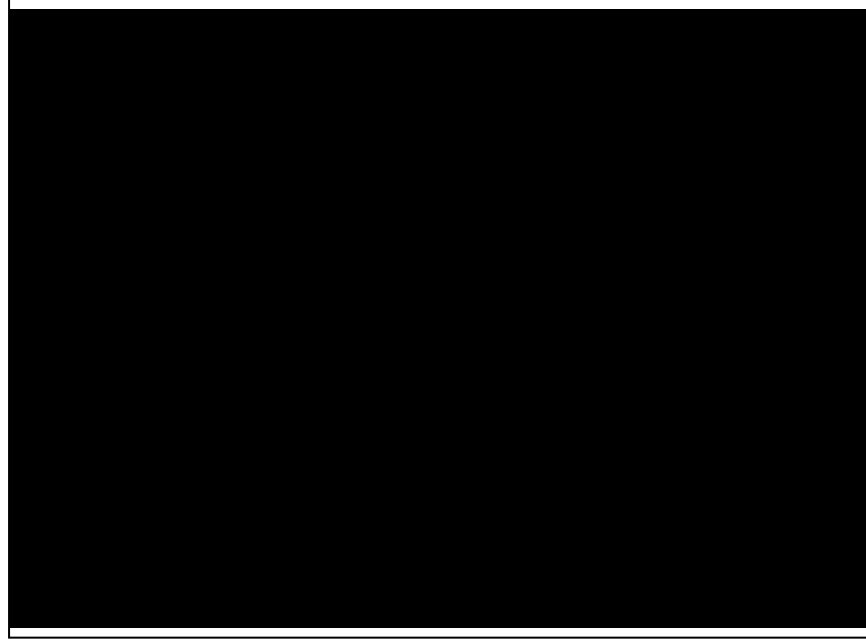
Cation transport within the polymer is calculated with the Nernst-Planck equation

$$\frac{\partial c}{\partial t} - \nabla \cdot (D \nabla c + z\mu Fc \nabla V) = 0 \quad (4.1)$$

where  $c \in \mathbb{R}$  is the cation concentration,  $D$  is the diffusion coefficient,  $F$  is the Faraday constant,  $z$  is the charge number,  $\mu$  is the cation mobility, and  $V \in \mathbb{R}$  is the electric potential in the polymer. It should be noted that in this model, cation migration is strictly driven by the presence of a potential gradient and the concentration gradient. This simplification can be made by comparing the pressure gradient  $\mu c \Delta V \nabla P$  with the electric potential gradient  $\mu c F \nabla V$ . The both share  $\mu c$ , so these terms can be neglected; however, looking at the other coefficient, it can be observed that  $F = 96,485 \frac{C}{mol}$  and  $\Delta V \approx 6 \times 10^{-6}$ , and so we can see that  $|F \nabla V| \gg |\Delta V \nabla P|$ , thus the contribution from the pressure gradient is negligible for the actuation model.

Applied voltage causes all free cations to migrate towards the cathode. Since the anions are fixed to the polymer backbone, the equation solves for strictly cation concentration.

Table 4.1. Values of constant expressions.



Because cations cannot leave the polymer domain, concentration begins to converge near the electrode polymer interface. This in turn increases the electric field.

$$-\nabla^2 V = \frac{\rho_s}{\epsilon_0 \epsilon_r} \quad (4.2)$$

where  $V$  is considered to be the potential in the polymer, and  $\epsilon_0 \epsilon_r$  is the dielectric permittivity. The dielectric permittivity is explicitly expressed in the simulations as  $\epsilon_0 \epsilon_r = \epsilon$  where  $\epsilon_0$  is the dielectric constant in a vacuum and  $\epsilon_r$  is the relative permittivity. The space charge density is defined in order to affect the electric field as follows

$$\rho_s = F(c - c_0) \quad (4.3)$$



where  $c_0$  is assumed the constant anion concentration. The value for anion concentration and dielectric permittivity are given in table 1. In this study, the electric field propagation down the electrode length is simplified. Rather than using Ohm's law to determine the electric current propagation, the electrode domain was partitioned near the location of the voltage source. This implementation was used in order to simplify the electrodynamics in order to investigate the solid mechanics more effectively. The electrode surface is still taken into consideration because the platinum domain stiffness cannot be neglected when analyzing the solid mechanics. It should be noted that, typically, the diffusion equation and the Poisson's equation could be solved for analytically by deriving a Green's function; however, this novel method of physical modeling causes this method to ineffective. The source terms driving both equations are continuously dependent on the solution of one another. This, in turn causes nonlinearities in the equations, which in turn necessitates the implementation of the finite element method. This will be further elaborated in Appendix A.

### **Mechanics Model**

In order to link the deflection with the cation transport, force coupling similar to that shown in Ref. 1 is used. A basic linear elastic model was used in order to quantify the mechanical behavior of the IPMC. The following equation describes the strain relationship with respect to the deformation

$$\boldsymbol{\epsilon} = \frac{1}{2}(\nabla \mathbf{u}^T + \nabla \mathbf{u}) \quad (4.4)$$

where  $\epsilon \in \mathbb{R}^{6 \times 6}$  is the strain tensor, and  $\mathbf{u} \in \mathbb{R}^3$  is the displacement vector. It can be seen that this generalization of strains implies that strain components are of the form  $\epsilon_{ij} = \frac{1}{2} \left( \frac{\partial u_i}{\partial x_j} + \frac{\partial u_j}{\partial x_i} \right)$ , thus strains in the normal direction are of the form  $\epsilon_{ii} = \frac{\partial u_i}{\partial x_i}$ .

If the differential operator is expressed in matrix  $\mathbf{D}$  form rather than a gradient operator  $\nabla$ , the Cauchy strain tensor can be expressed in matrix form as follows

$$\begin{bmatrix} \epsilon_{11} \\ \epsilon_{22} \\ \epsilon_{33} \\ \epsilon_{12} \\ \epsilon_{23} \\ \epsilon_{13} \end{bmatrix} = \begin{bmatrix} \frac{\partial}{\partial x} & 0 & 0 \\ 0 & \frac{\partial}{\partial y} & 0 \\ 0 & 0 & \frac{\partial}{\partial z} \\ \frac{\partial}{\partial y} & \frac{\partial}{\partial x} & 0 \\ \frac{\partial}{\partial z} & 0 & \frac{\partial}{\partial x} \\ 0 & \frac{\partial}{\partial z} & \frac{\partial}{\partial y} \end{bmatrix} \begin{bmatrix} u \\ v \\ w \end{bmatrix} \quad (4.5)$$

which can then be expressed as

$$\epsilon = \mathbf{D} \mathbf{u} \quad (4.6)$$

The stress strain relationship is noted by the following equation

$$\sigma = \mathbf{E} \epsilon \quad (4.7)$$

where  $\sigma \in \mathbb{R}^{6 \times 6}$  represents the general stress tensor for three dimensional space,  $\mathbf{E} \in \mathbb{R}^{6 \times 6}$  is the elastic stiffness matrix. This simulation implements a standard linear elastic model for the solid mechanics, thus the stiffness matrix is explicitly of the following form

$$\mathbf{E} = \frac{E}{(1+\nu)(1-2\nu)} \begin{bmatrix} 1-\nu & \nu & \nu & 0 & 0 & 0 \\ \nu & 1-\nu & \nu & 0 & 0 & 0 \\ \nu & \nu & 1-\nu & 0 & 0 & 0 \\ 0 & 0 & 0 & (1-2\nu) & 0 & 0 \\ 0 & 0 & 0 & 0 & (1-2\nu) & 0 \\ 0 & 0 & 0 & 0 & 0 & (1-2\nu) \end{bmatrix} \quad (4.8)$$

where  $E$  is the elastic Young's modulus, and  $\nu$  is the Poisson's Ratio. Thus equation (4.7)

explicitly becomes

$$\begin{bmatrix} \sigma_{11} \\ \sigma_{22} \\ \sigma_{33} \\ \sigma_{12} \\ \sigma_{23} \\ \sigma_{13} \end{bmatrix} = \frac{E}{(1+\nu)(1-2\nu)} \begin{bmatrix} 1-\nu & \nu & \nu & 0 & 0 & 0 \\ \nu & 1-\nu & \nu & 0 & 0 & 0 \\ \nu & \nu & 1-\nu & 0 & 0 & 0 \\ 0 & 0 & 0 & (1-2\nu) & 0 & 0 \\ 0 & 0 & 0 & 0 & (1-2\nu) & 0 \\ 0 & 0 & 0 & 0 & 0 & (1-2\nu) \end{bmatrix} \begin{bmatrix} \epsilon_{11} \\ \epsilon_{22} \\ \epsilon_{33} \\ \epsilon_{12} \\ \epsilon_{23} \\ \epsilon_{13} \end{bmatrix} \quad (4.9)$$

By this formulation, the volumetric force equation can be described at equilibrium as follows

$$-\mathbf{D}^T \boldsymbol{\sigma} = \mathbf{F}_V \quad (4.10)$$

Where  $\mathbf{F}_V \in \mathbb{R}^3$  represents the body force per unit volume. Since the divergence of a second order tensor field produces a first order tensor, the following equation becomes equivalent.

$$-\nabla \cdot \boldsymbol{\sigma} = \mathbf{F}_V \quad (4.11)$$

Where the divergence is defined for the second order tensor as

$$\nabla \cdot \boldsymbol{\sigma} = \begin{bmatrix} \frac{\partial \sigma_{11}}{\partial x} + \frac{\partial \sigma_{12}}{\partial y} + \frac{\partial \sigma_{13}}{\partial z} \\ \frac{\partial \sigma_{12}}{\partial x} + \frac{\partial \sigma_{22}}{\partial y} + \frac{\partial \sigma_{23}}{\partial z} \\ \frac{\partial \sigma_{13}}{\partial x} + \frac{\partial \sigma_{23}}{\partial y} + \frac{\partial \sigma_{33}}{\partial z} \end{bmatrix} \quad (4.13)$$

For the transient case, the equation becomes of the form

$$\rho \frac{\partial^2 \mathbf{u}}{\partial t^2} - \nabla \cdot \boldsymbol{\sigma} = \mathbf{F}_V \quad (4.15)$$

where  $\rho$  is the mechanical density, which is being multiplied by the transient term in the mechanical equation. By getting the stress in terms of deformation, the explicit equation for displacement then becomes

$$\rho \frac{\partial^2 \mathbf{u}}{\partial t^2} - \mathbf{D}^T \mathbf{E} \mathbf{D} \mathbf{u} = \mathbf{F}_V \quad (4.16)$$

Ref. 1 defines the body force in one direction as

$$\mathbf{F}_V = (\alpha \rho_s + \beta \rho_s^2) \hat{x} \quad (4.17)$$

Where  $\alpha$  and  $\beta$  are empirically found constants [1]. It was proposed by Pugal that the calculation of the body force should be implemented more precisely in 3D by the following equations

$$\mathbf{F}_{V;cathode} = \alpha \rho_s^2 \quad (4.18a)$$

$$\mathbf{F}_{V;anode} = \beta \rho_s \quad (4.18b)$$

where the quadratic term applies only to the neighborhood about the cathode and the linear term applies to the neighborhood about the anode. The issue with the implementation of this force coupling model is that it requires previous knowledge about where the potential is being applied. This is not necessarily the case for the design optimization. In some cases, the applied voltage location is used as a variable in order to produce an optimal design output. In order to correct the direction for three-dimensional implementation as well as maintain robust consistency when running design optimization, the original equation was augmented as follows

$$\mathbf{F}_V = \frac{\nabla c(\alpha\rho_s + \beta\rho_s^2)}{|\nabla c|} \quad (4.19)$$

where  $\nabla c \in \mathbb{R}^3$  is the concentration gradient. In vector form, this becomes the following

$$\mathbf{F}_V = \frac{(\alpha\rho_s + \beta\rho_s^2)}{\sqrt{\left(\frac{\partial c}{\partial x}\right)^2 + \left(\frac{\partial c}{\partial y}\right)^2 + \left(\frac{\partial c}{\partial z}\right)^2}} \begin{bmatrix} \frac{\partial c}{\partial x} \\ \frac{\partial c}{\partial y} \\ \frac{\partial c}{\partial z} \end{bmatrix} \quad (4.20)$$

This method was used to direct the body force appropriately. This is done by normalizing the magnitude of the concentration gradient while maintaining the direction.

### **Finite Element Implementation**

The mathematical equations tabulated were solved for using the Finite Element Method. These calculations were carried out in a finite element software package known as COMSOL MULTIPHYSICS. The IPMC modeled in this study is a Nafion based membrane that is coated with a layer of platinum. The IPMC was modeled as concentric cylinders. The polymer domain was constructed with an outer diameter 1[mm] and the platinum layer was .1[mm] thick. The IPMC was constructed to be 25.4[mm] long.

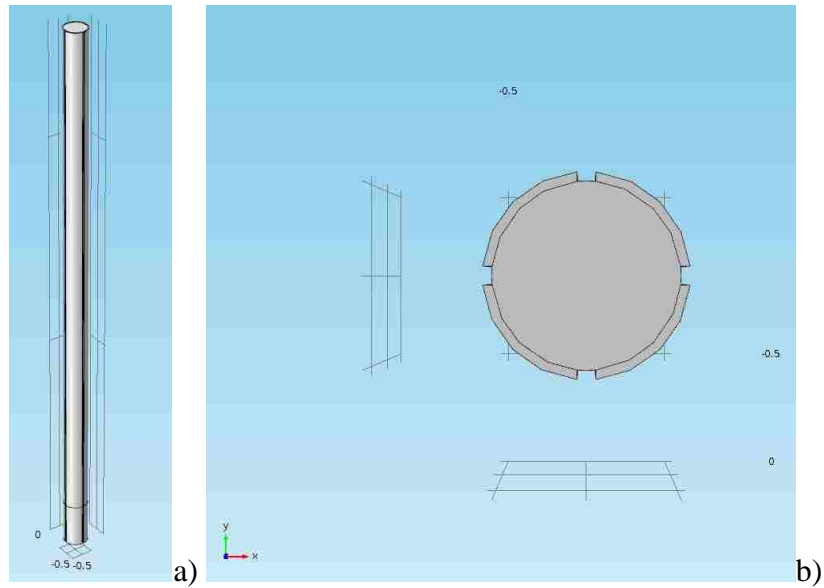


Figure 4.1. Initial IPMC Geometry a) isometric view b) cross-section view

It can also be noticed in that there is a small partition along the platinum domains near the base of the IPMC. These are the boundaries that the source potentials will be applied to. They are used to simulate the clamps that hold the IPMC.

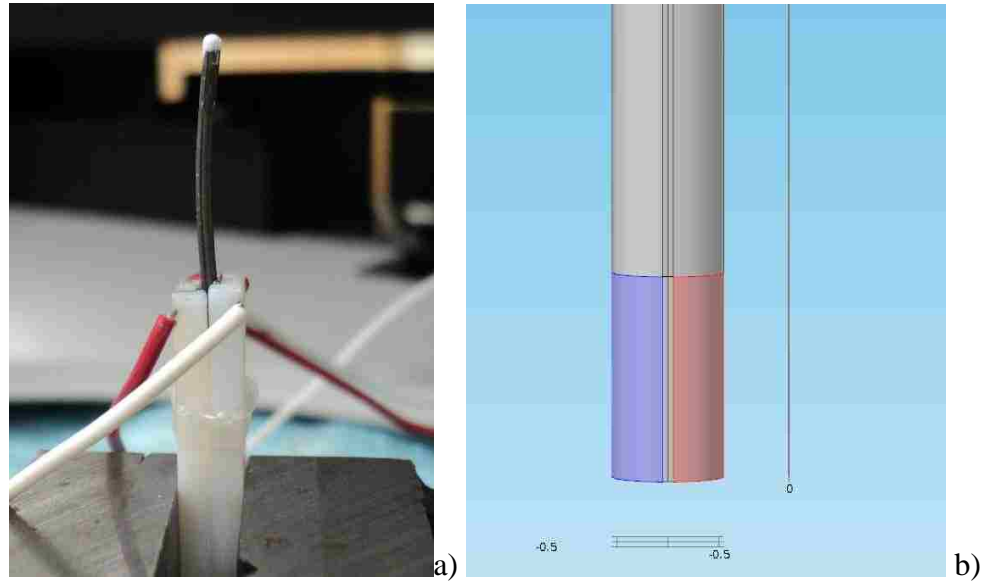


Figure 4.2. Clamp boundaries a) Experimental b) Simulated

These clamps are used to simulate the location where the voltage is being applied as well as the effective distance that the voltage propagates [1]. The boundaries to the left are the locations of the applied voltages, and the boundaries to the right are the locations of the grounded voltages. This is easier to see with a cross sectional view.

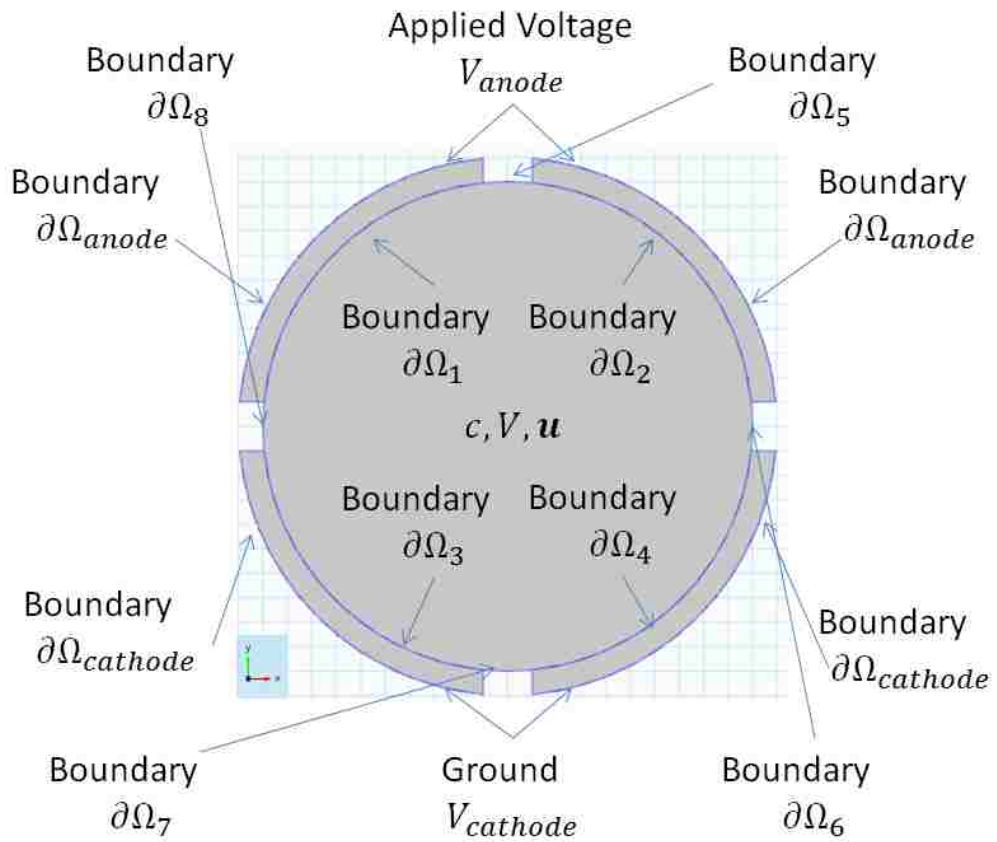


Figure 4.3. Cross sectional description of the boundaries

The simulation would simultaneously solve Eqs. (4.1), (4.2), and (4.15). The following is a list of boundary conditions used to run simulations. It is to be assumed that with the exception of the potential boundaries that are applied up to the clamp extension, all other boundary conditions extrude throughout the length of the IPMC.



- For Eq (1) in the polymer domain:

$$-(D \nabla c + z\mu Fc \nabla V) = 0 \quad (4.21)$$

This insures that cations cannot leave the polymer domain.

- For Eq (2), In the polymer domain

- Anode boundary

$$V_{\partial\Omega_1, \partial\Omega_2} = V_{anode} \quad (4.22)$$

- Cathode boundary

$$V_{\partial\Omega_3, \partial\Omega_4} = V_{cathode} \quad (4.23)$$

- Other boundaries

$$N \cdot \nabla V = 0 \quad (4.24)$$

- For Eq (3), In both domains

- Entire face boundary

$$\mathbf{u} = 0 \quad (4.25)$$

### **Mesh-Optimization**

The mesh resolution plays a significant role in both the computational time as well as the model accuracy. COMSOLs default mesh builder is a physics based mesh builder which constructs a mesh based on triad elements. This can be seen explicitly in the Figure 4.4.

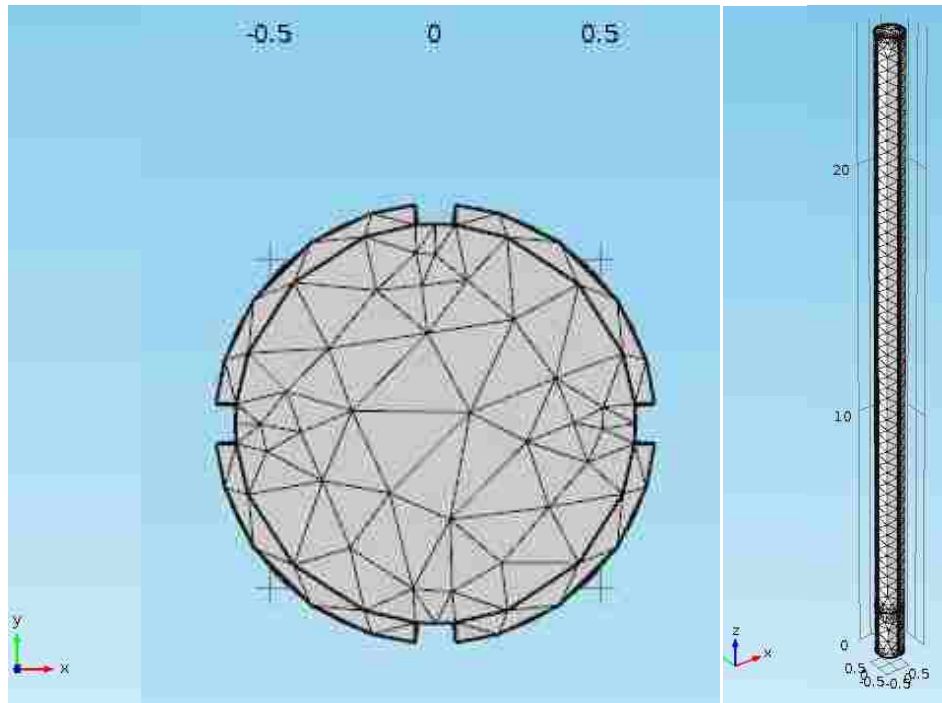


Figure 4.4. Finite element Normal Physics based mesh

There are many undesirable results from the default mesh. The first issue that could be noticed is along the length. The mesh resolution here is pretty high, and the solid mechanics do not necessitate this degree of resolution for the bending. This adds to the computational complexity. The face is also very coarse near the electrode-polymer interface. This becomes an issue when measuring the cation concentration. Near this interface, a boundary layer begins to form based on the concentration. If the mesh on the face is too coarse, the concentration will be measured as values lower than they should be. Lastly, the physics driven mesh has issues constructing a continuous mesh near the clamp boundaries.

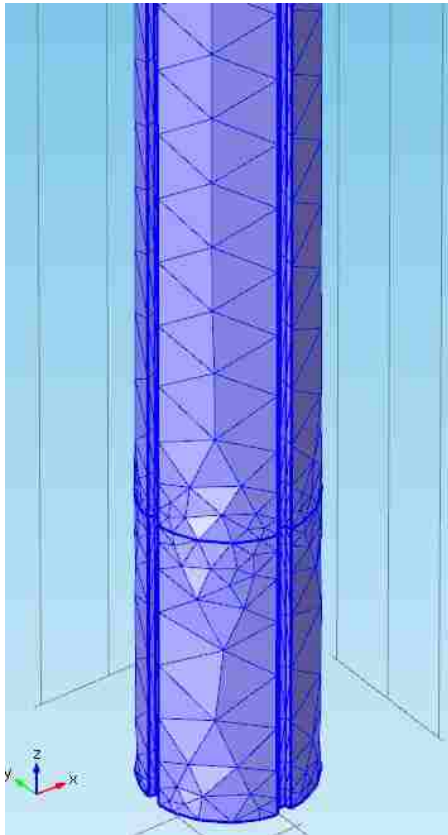


Figure 4.5. Normal Physics based mesh near the clamp domain

This strange construction becomes an issue for the solid mechanical studies. The deflection near this location becomes unstable due to the large aspect ratios that become local to the clamp boundaries.

The first method used to address these issues required manually constructing a user defined mesh. This mesh was constructed by first creating a free triangular mesh on the circular face of the IPMC geometry.

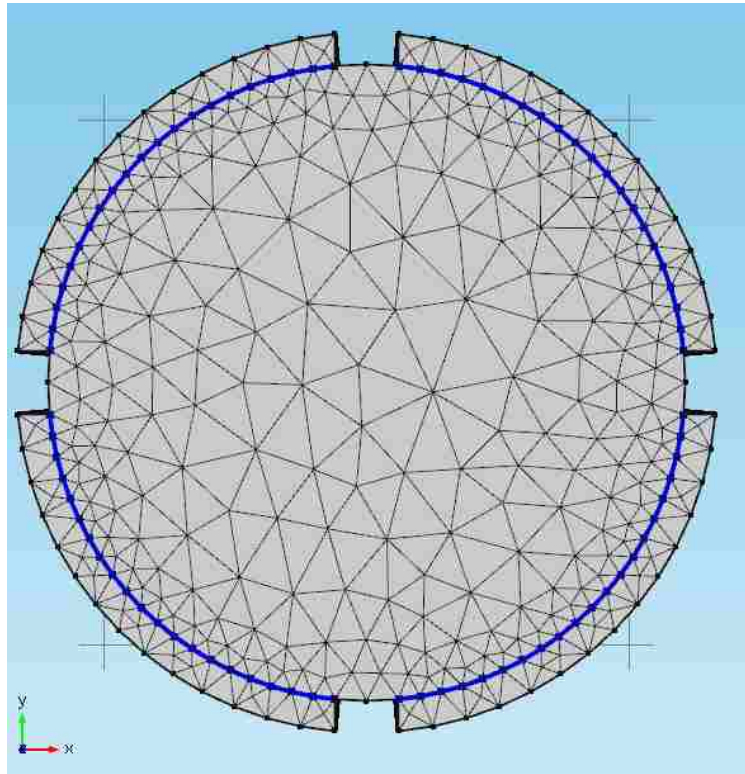


Figure 4.6. User Defined Mesh with edge distribution

The free triangular mesh on the face was refined by constructing a distribution along the polymer-electrode interface. This distribution segmented the arc edges into twenty straight edges. This was the only governing guideline for meshing the face. This allowed the mesh resolution to be high near the interface and coarse far away from the mesh. This can be seen in figure 4.6

The triangular mesh was then extruded down the length to construct a mesh based on triangular prisms. This extrusion was coarse down the length because the mesh resolution required for the solid mechanics at this length is not incredibly fine. By minimizing the number of elements allows for quick computations. This mesh can be seen in Figure 4.7.

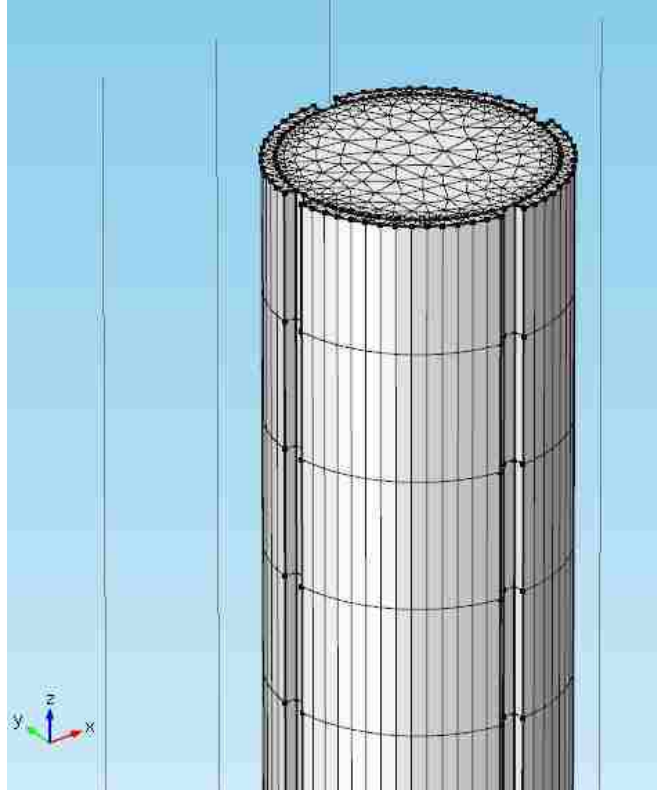


Figure 4.7. User Defined Mesh Extrusion

This manual construction of the mesh was also helpful in maintaining mesh continuity along the length. The aspect ratio at the clamp boundary is now fixed. This can be seen in figure 4.8.

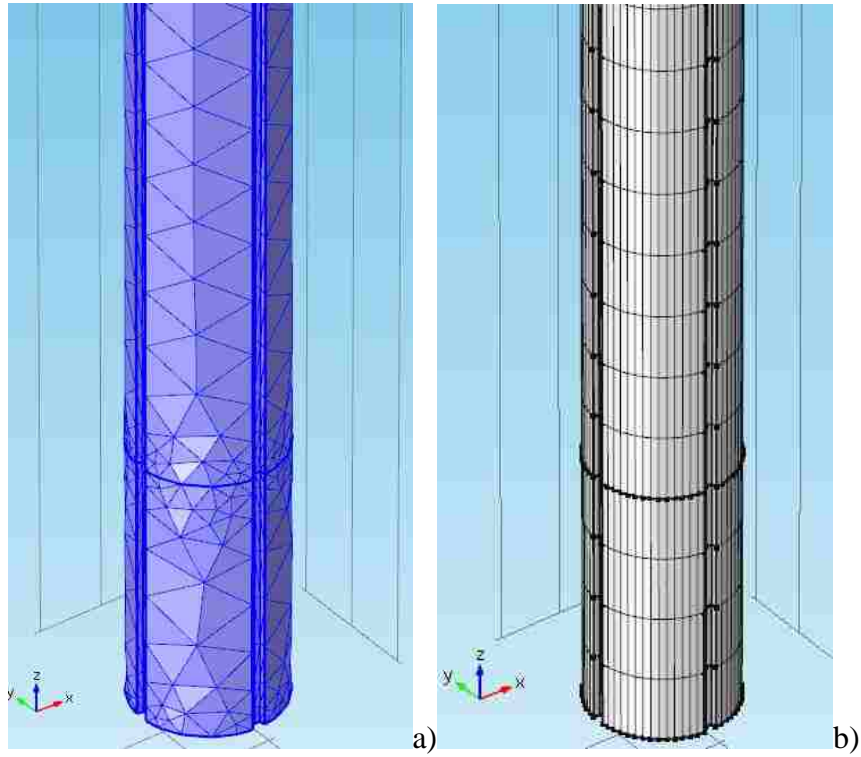


Figure 4.8. Clamp boundary comparison a) Default mesh, b) Manual mesh

When we compare the results from the two meshes, we can see that the variance is significant. The magnitudes of the maximum concentration between the two simulations are fairly different by about  $300 \frac{\text{mol}}{\text{m}^3}$ . The concentration distribution seems significantly different as well. This is because of the boundary layer that is developed by the concentration. These comparison results can be seen in figure 4.9.

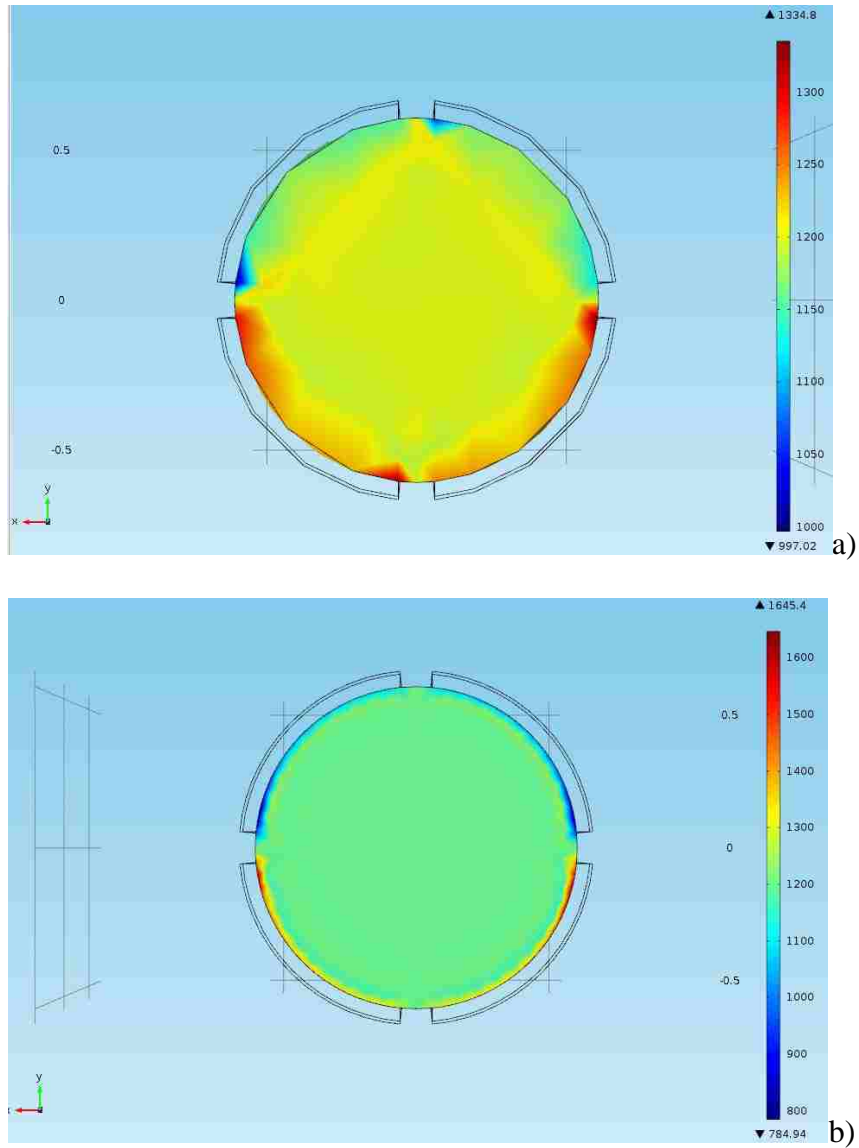


Figure 4.9. Concentration comparison a) Default mesh, b) Manual mesh

Though this mesh refinement provides more physically accurate results, the time necessary for each simulation result is 2 hours. When considering the design optimization, it will be necessary to simplify the model in order to produce some timely results. By manually constructing the mesh in a similar manner and augmenting the force

coupling coefficients, it is viable to construct a more course mesh and still produce desirable results. Figure 4.10 is demonstrates the mesh used for the design optimization.

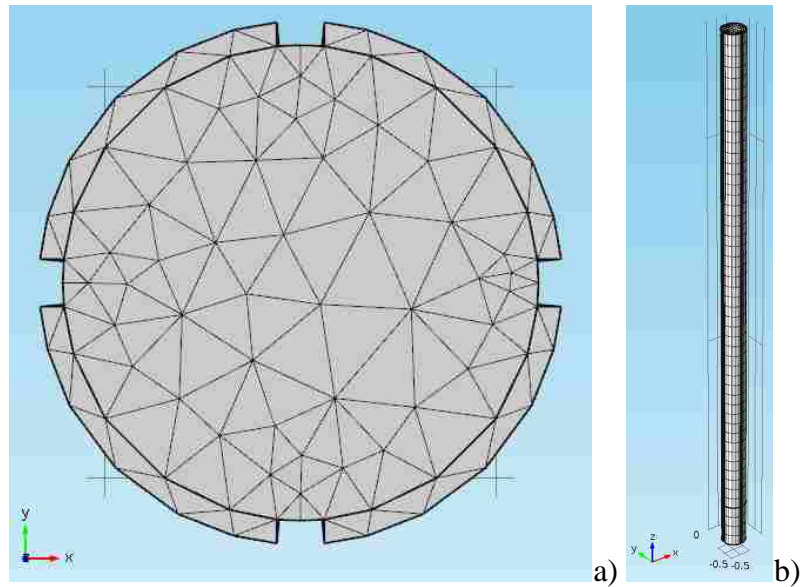


Figure 4.10. Finite element mesh a) Triangular mesh b) Swept mesh

With this manual mesh still produces better results than the default mesh; however, the concentration is still not as accurate as the previously tabulated mesh. The concentration results of this mesh can be seen in figure 4.11



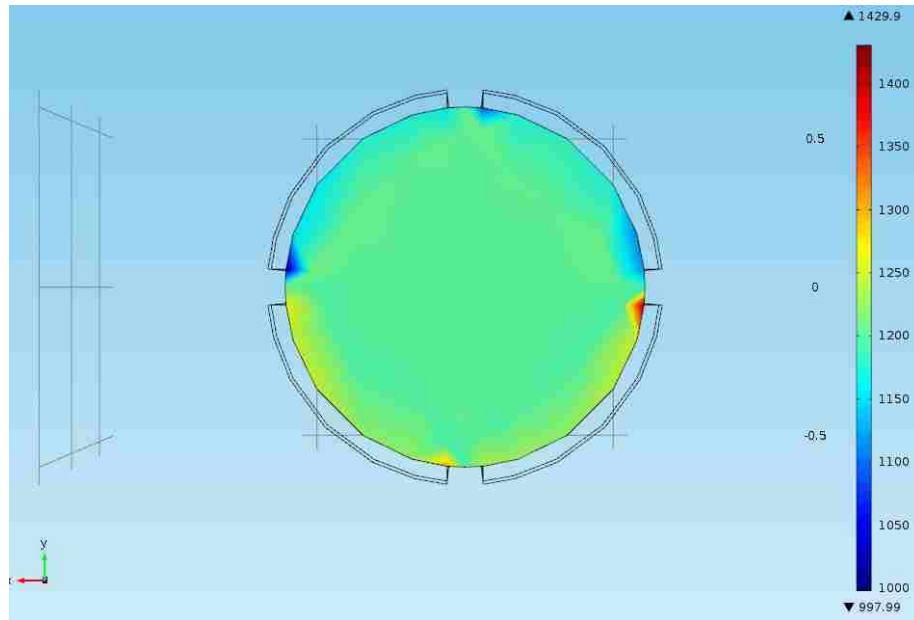


Figure 4.11. Concentration results for the design optimization mesh

### **End-Effector Displacement**

An empirical study had to be conducted in order to confirm the validity of the computational model. During this study, a physical rod type IPMC was actuated with a voltage source of 1V. The end-effector displacement was measured using a microscope camera tracking the tip displacement. A white marker is used on the tip in order to allow the computer to distinguish the tip from the rest of the IPMC and the back drop. A small black piece of construction paper was placed around the IPMC in order to have a consistent color throughout the background. The displacement was tracked for a constant voltage for 30 seconds. Using the same boundary conditions, a constant voltage of 1V was applied to the clamp domain of the IPMC for thirty seconds.

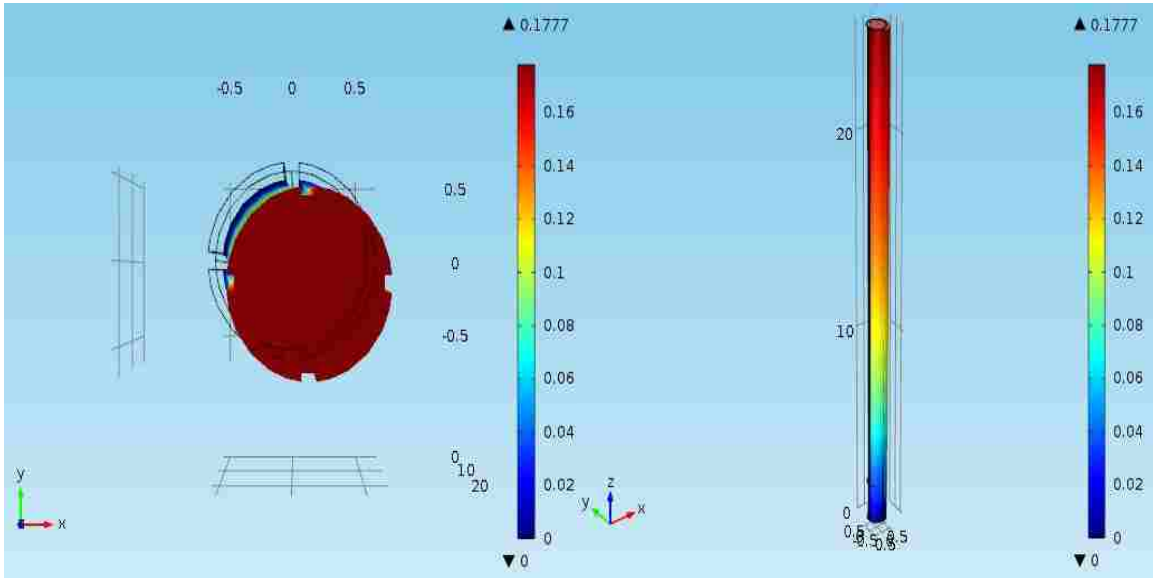


Figure 4.12. Image of the end-effector displacement for the IPMC

The results for the motion tracking were noisy, so a logarithmic curve was used to fit the data and compare to the finite element results. A direct comparison can be seen in Fig 9. The dynamic response of the end-effector displacement initially starts lagged in comparison to the experimental data; however the two act characteristically similar after around 5 seconds. This could be due to exaggerated noise producing artifacts in the data that make the simulation seem lagged.

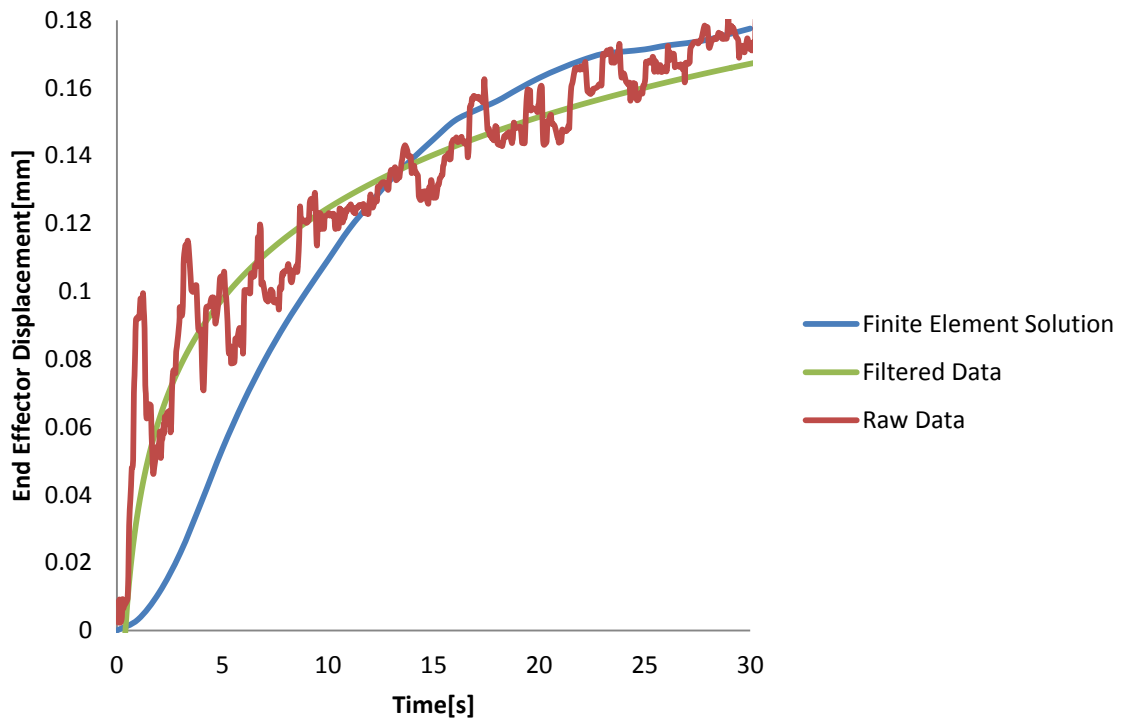


Figure 4.12. Tip displacement vs time comparison

After 5 seconds, the empirical findings match characteristically with the finite element results. The overall magnitudes of the displacements are within the tolerance of micron displacements, therefore the finite element simulations are accurate at determining the mechanical displacements of the end effector. This time delay might also be an issue of the boundary layer where a bulk of the concentration converges. This might occur at a much faster rate provided a finer mesh; however, this would drastically increase the computational time required to run the simulation.

## **Discussion**

The explicit method of modeling the IPMC actuation yields some promise for the rod type. This is due to a number of factors. For one, the rod type is so thick that the deformation could still be accurately captured without having to resort to a large deformation model. The explicit model also captures many parameters that could not be altered given the RC model, such as the explicit cation transport, the electric field, and the explicit geometric representation of the IPMC. This is even more attractive when conducting design optimization in the sense that all of the physical parameters can be analyzed thoroughly in order to determine which design parameters are more sensitive than others in order to determine ideal designs. This model is fairly intuitive to construct, and utilizing COMSOL MULTIPHYSICS provides some clear explicit results. Lastly, because this model is entirely physics based, the explicit results are more reliable than the results from the lumped RC simulations. Cation transport is no longer bounded by the discrete partitions of the IPMC, thus some of the previous notions of IPMC actuation can be disproven with this model.

One downside with the explicit physics model is that it requires a tremendous amount of computational power. Assumptions had to be made about the electrical field conducting down the length in order to produce some timely results. This computational issue could potentially be resolved by sending jobs to a supercomputer or a cluster; however, this would also require another license file as well as a specific compiler. Another potential obstacle as far as the explicit model is concerned is implementing a feedback controller that accurately models the system for practical use. Analytic controllers will not work on a multiphysics system like this one. Fortunately, this simulation could be coupled with

software packages such as MATLAB. In principle, by linking COMSOL MULTIPHYSICS to SimuLink through Live Link with MATLAB, a numerical feedback controller could be implemented with more accurate results as well as methods as how to design a controller for an IPMC for practical purposes.

## **CHAPTER 5: DESIGN OPTIMIZATION**

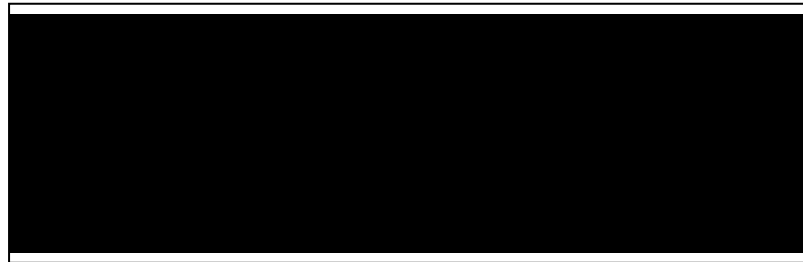
This chapter will utilize a multi-physics approach to develop optimized designs for a 3D actuation model for the IPMC. The optimization will be conducted through a software package known as COMSOL MULTIPHYSICS. By using the explicit physics method previously tabulated, this study will provide three designs that could be used for three optimal outputs. The first study will be conducted to find an optimal diameter in order to maximize the end-effector bending for the IPMC actuator. The second study will be conducted by optimizing the diameter in order to maximize the force transmission from an IPMC actuation device. Lastly, the electrical potential of an eight electrode rod type IPMC will be optimized in order to induce twisting about the axis of its extrusion. A brief discussion will be made in regards to potential inconsistencies as well as potential methods to make the model more accurate.

### **Optimization Implementation**

Conceptual designs can be constructed through optimization of the finite element model. The main objective of the design optimization is to run three separate optimization studies. The first study is conducted in order to maximize the top displacement with respect to changes in the rod thickness. The second study is performed in order to

optimize the volumetric body that drives the deflection with respect to the rod thickness. The final study determines the optimal voltage configuration for an alternative electrode pattern necessary to maximize rotation about the axis of cross sectional extrusion, or the length. In order to create augmented designs, design parameters must first be established. Initial design parameters are tabulated in Table 2.

Table 5.1 Initial values of parameter expressions.



The entire geometry was constructed with the tabulated parameters. By parameterizing the geometry, it is possible to treat the geometry as a dependent variable for the physical model.

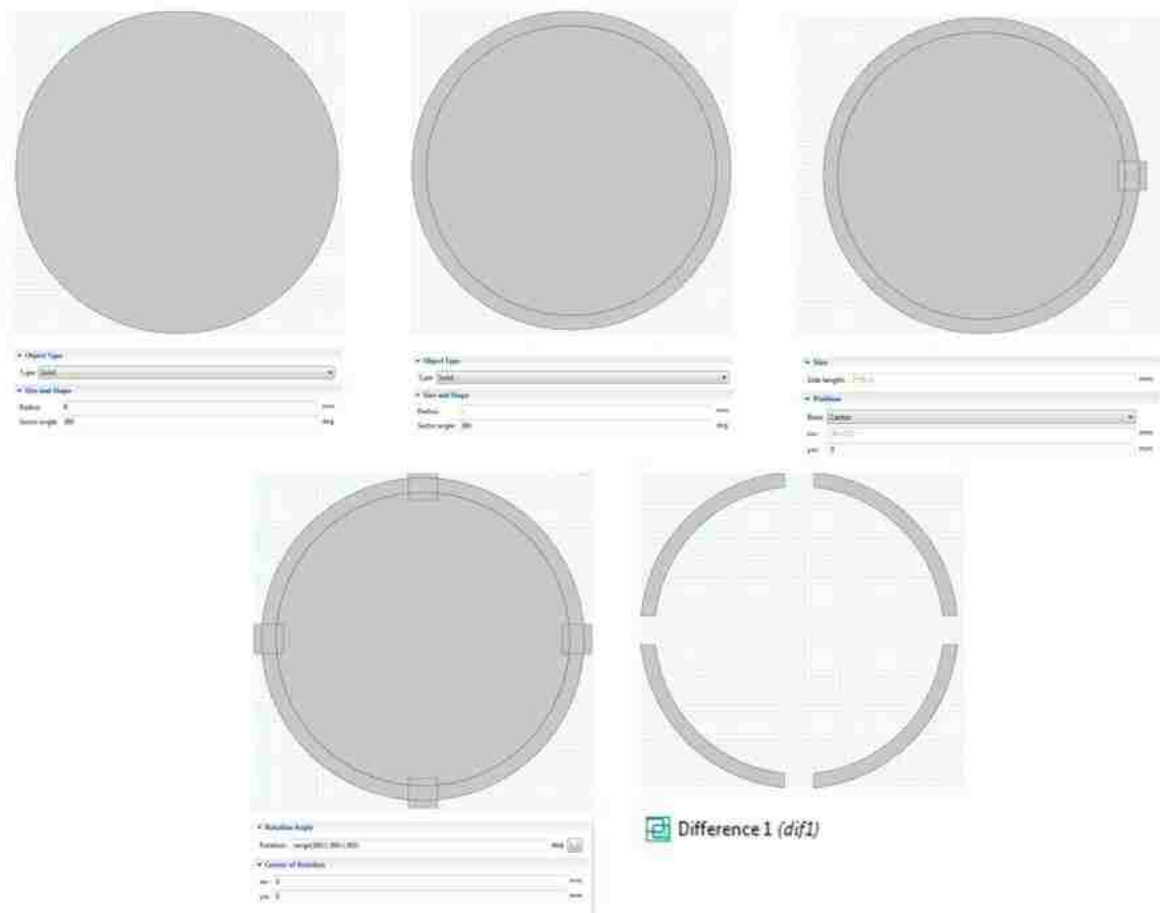


Figure 5.1. Parametrized construction of the electrode domains

For the three different optimization studies, three different probes were used as feedback values to be used. For the first study, a boundary probe was used at the polymer face of the end-effector. The boundary probe read the maximum displacement at the end-effector tip,  $\|\mathbf{u}\|_{\infty}$ . For the second study, a domain probe was used in the polymer domain. This probe was used to measure the maximum space charge density,  $\|\rho_s\|_{\infty}$ . This is used in order to maximize the force production of an IPMC actuator. Since the volumetric body force of an IPMC is defined by Eq. 10, it is can be seen that maximizing the space charge



density would produce an optimal force value. For the final study, a domain probe was used in the polymer domain near the clamps. This probe retrieves the maximum value of the curl displacement about the z-axis,  $\left\| \gamma_{xy} \right\|_{\infty}$ . This is used to maximize the twisting motion about the axis of extrusion. By defining these parameters, the design optimization problem becomes more apparent as can be seen in Fig. 7.

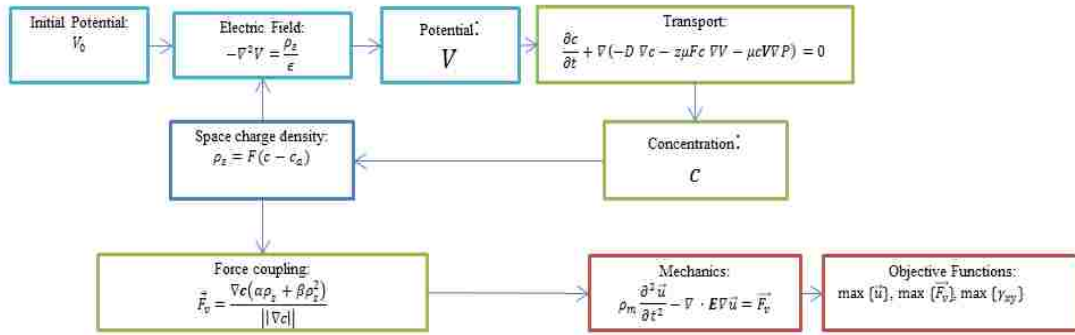


Figure 5.2. Block diagram detailing dependent multi-physics phenomenon

Optimization was also conducted in COMSOL MULTIPHYSICS. The Nelder-Mead method of least squares was used to find maximum values for the objective expressions. The probes were used as the objective expressions for each of the studies. The studies are conducted in order to maximize the objective expressions.

## **Optimal Radius for End-Effector Displacement**

For the maximization of end-effector displacement, the initial values of the parametric expressions are as tabulated in Table 2. The voltages were fixed and applied on the top two electrodes at the clamp boundaries. The bottom two electrode clamps were treated as grounds. The variable parameter used in this study was the IPMCs radial thickness. The outer radius was allowed to vary from a range of .11[mm] to 1.1[mm]. This range was decided to be the extreme limits that an IPMC thickness can be seeing as how flat IPMCs have a thickness 180 microns<sup>1</sup>. Transient studies were conducted for 1second intervals and displacements were measured from this. The results of the end-effector optimization can be seen in Fig. 10. The optimization solver reduced the radius of the IPMC down to .11[mm], which is the minimum allowed IPMC radius for the study. This would inherently reduce the stiffness based on the spatial dimension, and allow the IPMC to bend more effectively.

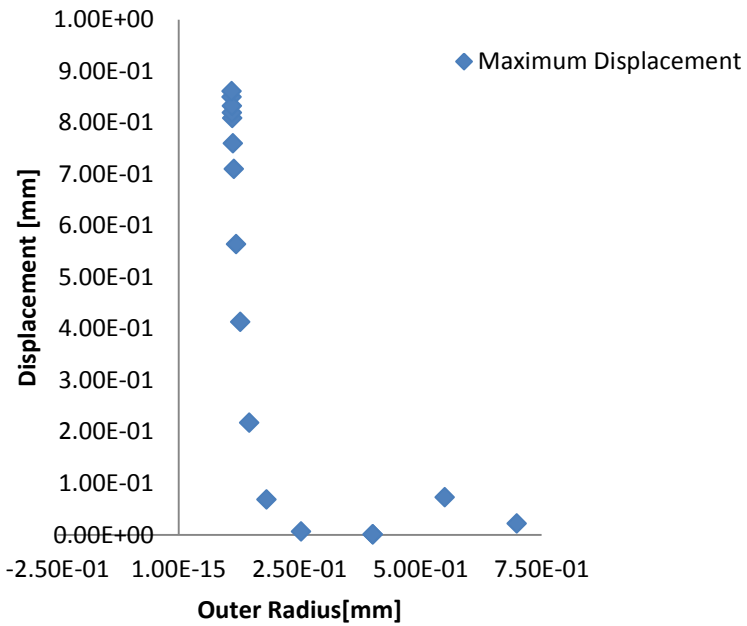


Figure 5.3. Optimal radius for maximum tip displacement

For end-effector deflection, it appears that the IPMC thickness can be arbitrarily small in order to design an actuator with more effective bending properties. The magnitude of the near instantaneous deflection increased more than ten times by reducing the thickness to a fifth of its original size.

### **Optimal Radius for Force Output**

In order to maximize the force output, it is necessary to maximize the volumetric body force that drives the IPMC. Since the volumetric body force is defined by Eq.10, it suffices to optimize the space charge density in order to maximize the body force, thus maximizing the output force. For the maximization of output force, the initial values of

the parametric expressions are as tabulated in Table 2. The voltages were fixed and applied on the top two electrodes. The bottom two electrodes were treated as grounds. The variable parameter used in this study was the IPMCs radial thickness. The outer radius was allowed to vary from a range of .11[mm] to 1.1[mm]. The results of the space charge density optimization can be seen in Fig 11.

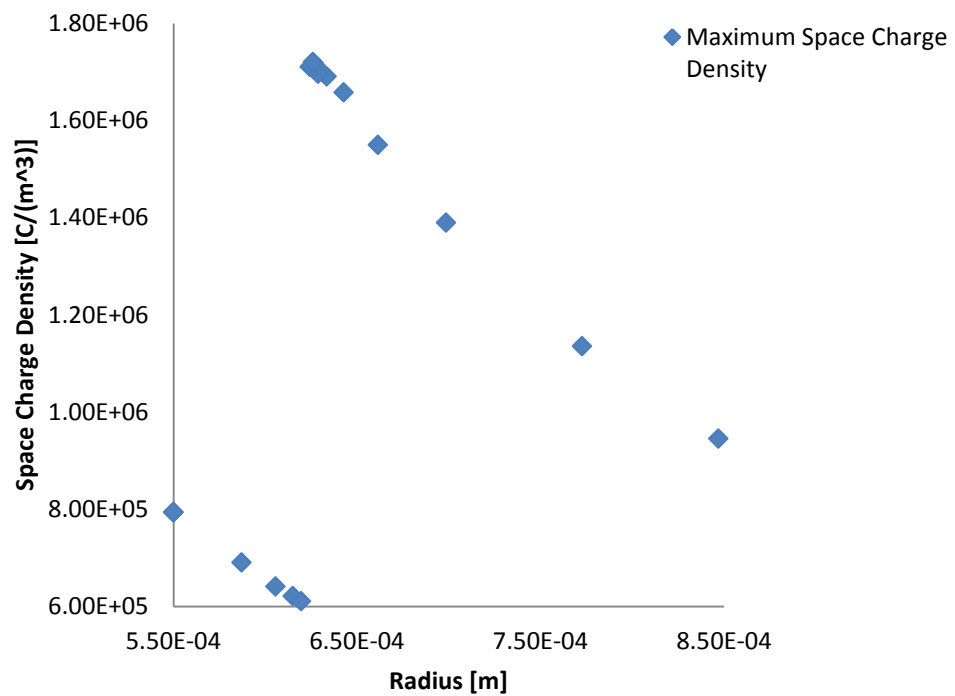


Figure 5.4. Optimal radius for maximum Space Charge Density

The maximum space charge density is achieved with an outer radius of .624[mm]. The significance of this result is that IPMCs cannot be made arbitrarily large in order to

produce an optimal force transmitter. There exist optimal values that maximize the space charge density, and since the force is a function of the space charge density, this means that there is an optimal force value. This also means that small changes in the thickness can produce large improvements in the force transmission. A radial increase of .07[mm] could potentially quadruple the force output.

### **Optimal Voltage Configuration for Twisting**

Given the four electrode configuration of the rod type IPMC, it is difficult to control the rotation about the z-axis. Electric potential sources result in fairly limited configurations as seen in Fig.1. Based on the results of Pugal and Kim, flat type IPMCs have the potential to rotate about their longitudinal axis by splitting the electrode on top and bottom<sup>1</sup>. This concept was applied to the rod type IPMC in order to conduct studies to determine optimal twisting about the longitudinal axis. By setting the  $i = 8$ , the geometry is then altered in order to split the electrodes. This produces a rod type IPMC with 8 electrode domains as seen in Fig 12.

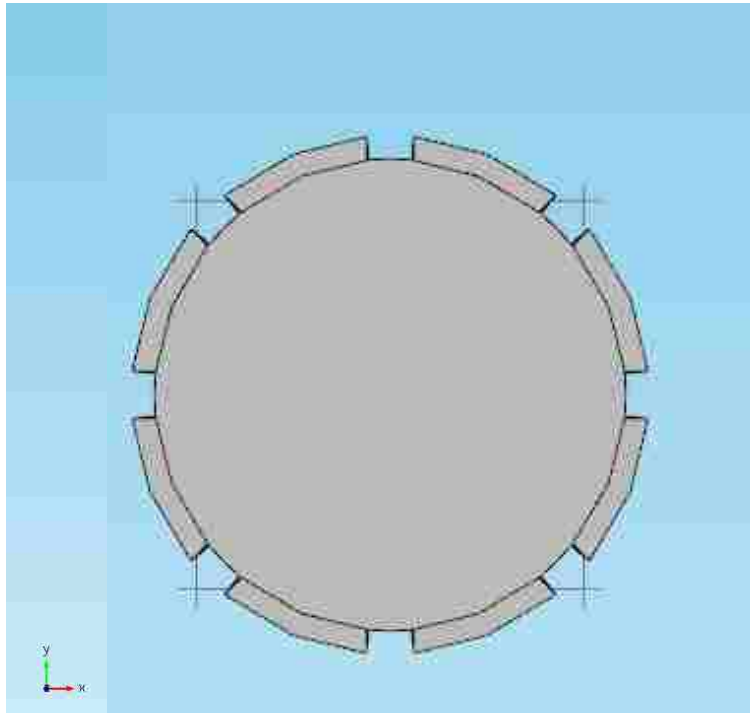


Figure 5.5. IPMC with 8 electrode domains

In principle, it should be conceivable for this design to produce twisting about its longitudinal axis. Each electrode clamp boundary was initiated at a source potential of .5V. They were allowed to vary from 0-1V. The radius was fixed for this study. The objective function that was chosen for analysis was the curl displacement about the Z-axis. This probe was located at the base near the clamp boundaries. The results of this can be seen in Table 5.2.

Table 5.2. Final Voltage Expressions in counter clockwork order.

V1	V2	V3	V4	V5	V6	V7	V8
.871[V]	.731[V]	.639[V]	.495[V]	.251[V]	.269[V]	1[V]	0[V]

This voltage configuration maximized the curl displacement for the system. The optimization results can be seen in Fig 13.

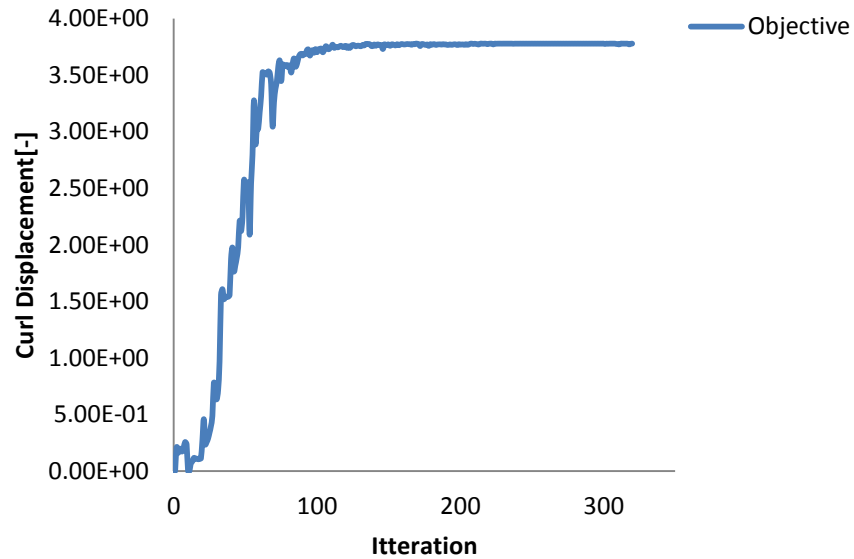


Figure 5.6. Curl Displacement Optimization

The twisting occurs through the deflection in the base of the IPMC. The overall magnitude of the deflection of the IPMC does not exceed 0.1043[mm]. This is localized

deformation near the base of the IPMC. This apparent expansion and compression in the base of the IPMC is the cause of the very small scale torsion that occurs within the IPMC.

This can be seen in Fig 5.7

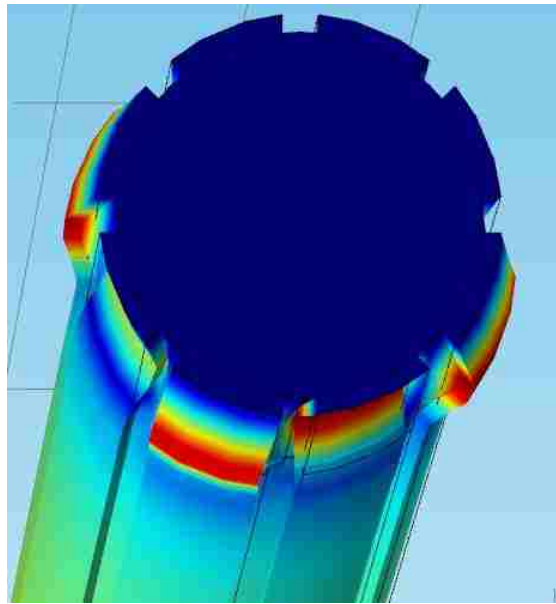


Figure 5.7.Compression and expansion

Although the twisting produced by the IPMC is not very pronounced, increasing the voltage magnitude could potentially allow the IPMC to get larger twisting magnitudes. This study still provides insight as to the normalized configuration that voltages should be applied in order to produce a valued output. The end-effector of the IPMC still moves, making the twisting seem even less significant; however, this is potentially beneficial. This ability to twist and bend allows IPMC to maneuver through obstacles; however, this result is still very circumstantial seeing as how the magnitude of the deflection is so slight.



## Discussion

The results from the optimization studies provide insight into steps that can be taken in the future development of rod type IPMC actuation devices. One of the main geometric considerations in this study was the rod thickness. In principle, it is possible to construct a rod type IPMC that can deflect at a desired magnitude by reducing its thickness. In theory, this physical representation should yield more accurate results due to the potential gradient becoming significantly larger than the induced pressure gradient created by the deflection<sup>1</sup>; however, due to the changing geometry, the mesh can become unstable. It is necessary to have active mesh refinement while running optimization. Large deflection could be a desirable attribute, but the manufacturing of IPMCs on the micron scale would be very difficult.

On the other end, the force optimization requires a slightly larger thickness than the typical IPMC. This result could become increasingly beneficial when attempting to construct machinery on a small scale. It should be kept in mind that the force coupling terms are determined empirically. Manufacturing of IPMCs with optimized force transmission would be inconsequential in comparison to the current IPMC dimensions.

Increased IPMC mobility is still within its adolescence; however, the potential for twisting IPMCs could become more valuable in the field of micro-machinery and invasive surgery. There are still computational considerations that will have to be taken into account. There is currently no means of validating these results. Empirical evidence can only be produced with a manufactured rod type IPMC with eight independent electrode surfaces. The fabrication of a cylindrical IPMC with eight electrodes would be a task within itself.

Future work could be put forth to seamlessly change in the electrode pattern for design optimization. Current issues reside in the boundary conditions becoming overlapped. This causes the simulations to produce faulty results that could become misleading to the optimization module. Simulations become increasingly time intensive when running mechanical simulations that augment the geometry. This could be solved for by running simulations on a supercomputer or a cluster. The proposed optimized designs still need empirical validation, and so fabrication of these designs will need to be technically addressed.

## CHAPTER 6: CONCLUSION

This thesis investigated many of the methodologies generally utilized in order to quantify the actuation of an IPMC. These actuation methods were implemented in order to quantify 3-dimensional actuation. With these actuation models, design optimization was implemented in order to more produce theoretical designs that could more properly perform tasks for a variety of end users.

The first model that was investigated was the lumped RC model. This method modeled the cation transport through the current flow in an RC circuit. The current was linked with the bending moment used in the model simulation. In the frequency domain, the input voltage could be directly linked to the input bending moment. The bending moment would then be applied to the large deformation model. The large deformation model was a dynamic model which does not assume rigid bodies. Utilizing beam elements to represent sectioned IPMCs and two lumped RC circuits in order to induce two bending moments, this model could represent bi-axial actuation. Even more so, this model could readily capture large deformation.

The second model that was investigated was the explicit physics model. This method explicitly models the cation transport under the influence of an electric field. This also effects the electric field simultaneously. The transport of cations drives the body load in the IPMC. This coupling causes the actuation within the IPMC. This explicit physics was

applied to a rod type IPMC in order to provide an actuation model. This model utilized a isotropic linear elastic model in order to model the solid mechanics. This limits the magnitude of deformation that the model can accurately capture; however, due to the thickness of the rod type IPMCs, the deflection is typically not large, thus the standard linear elastic model suffices to capture the actuation. This model also more accurately captures the physics within the system. This cation transport is allowed to propagate throughout the entire polymer domain, thus more providing more accurate insight to the actuation.

Lastly, design optimization was conducted using the Nedler-Mead least squares method. These studies were conducted on the explicit physics model in order to provide explicit designs. Three studies were conducted. The first study augmented the IPMC thickness in order to maximize the end-effector deflection. The second study augmented the IPMC thickness in order to maximize the transmitted force from an IPMC. The final study utilized an eight electrode IPMC. By augmenting the potential source, minor twisting was induced in the IMPC simulation.

Future work can build from this thesis could be to conduct studies on multiphysical models explicitly sectioned in a similar manner that the RC model is. Studies could also be conducted in methods to construct a theoretical feedback controller based on the explicit physics model. More hands on studies could be conducted in actually constructing IPMCs based on some of the designs provided from the optimization models.

There are still many factors regarding IPMCs that remain uncertain. These factors still limit the real-world applications of IPMCs. This study produced a simulation and design

optimization of a rod type IPMC utilizing first principles. A three dimensional finite element model was constructed that coupled transport phenomena, electrostatics, and solid mechanics. By doing so, it was possible to conduct optimization studies that could provide conceptual IPMC designs that would maximize deflection, force output, and twisting. These designs could become productive towards making devices which utilize IPMC actuation in a practical real world setting.

## APPENDIX A: GREENS FUNCTION SOLUTION FOR LINEAR PARTIAL DIFFERENTIAL EQUATIONS

Given  $\mathbf{x}$  and  $\boldsymbol{\xi} \in \mathbb{F}^n$  where  $\mathbb{F}$  is an arbitrary field, a linear differential operator  $\mathbf{D}$ , a function  $u(\mathbf{x}) \in W^{k,p}(\Omega)$  where  $W^{k,p}(\Omega)$  is a Sobolev space sufficiently defined for the operator  $\mathbf{D}$ , and such that the source terms of the function  $f(\mathbf{x})$ , such that the following equation is satisfied.

$$\mathbf{D}u(\mathbf{x}) = f(\mathbf{x}) \tag{A.1}$$

It is possible to derive a Green's function with the following formulation

$$\mathbf{D}G(\mathbf{x}, \boldsymbol{\xi}) = \delta(\mathbf{x} - \boldsymbol{\xi}) \tag{A.2}$$

where  $G(\mathbf{x}, \boldsymbol{\xi})$  is the Green's function, and  $\delta(\mathbf{x})$  is the Dirac delta distribution. It should be noted that  $\delta(\mathbf{x}) = \prod_{i=1}^n \delta(x_i)$ . By applying multiplying both sides of (A.2) by  $f(\mathbf{x})$  and integrating both sides, the following equation can be produced

$$\int_{\mathbb{F}^n} \mathbf{D}G(\mathbf{x}, \boldsymbol{\xi})f(\boldsymbol{\xi}) d\boldsymbol{\xi} = \int_{\mathbb{F}^n} \delta(\mathbf{x} - \boldsymbol{\xi})f(\boldsymbol{\xi}) d\boldsymbol{\xi} \tag{A.3}$$

since integration and differentiation are linear operators, (A.3) can be re-written as

$$\mathbf{D} \int_{\mathbb{F}^n} G(\mathbf{x}, \boldsymbol{\xi}) f(\boldsymbol{\xi}) d\boldsymbol{\xi} = \int_{\mathbb{F}^n} \delta(\mathbf{x} - \boldsymbol{\xi}) f(\boldsymbol{\xi}) d\boldsymbol{\xi} \quad (\text{A.4})$$

and since the Dirac delta distribution has the following properties

$$\int_{\mathbb{F}^n} \delta(\mathbf{x} - \boldsymbol{\xi}) f(\boldsymbol{\xi}) d\boldsymbol{\xi} = f(\mathbf{x}) \quad (\text{A.5})$$

(A.1) could be expressed as

$$\mathbf{D} \int_{\mathbb{F}^n} G(\mathbf{x}, \boldsymbol{\xi}) f(\boldsymbol{\xi}) d\boldsymbol{\xi} = f(\mathbf{x}) \quad (\text{A.6})$$

therefore, the fundamental solution is given as

$$u(\mathbf{x}) = \int_{\mathbb{F}^n} G(\mathbf{x}, \boldsymbol{\xi}) f(\boldsymbol{\xi}) d\boldsymbol{\xi} \quad (\text{A.7})$$

Though the principle is straight forward, the application becomes cumbersome. Deriving the greens function  $G(t, \mathbf{x})$  requires fairly difficult integral transformations; however, this method provides the fundamental solution to linear non-homogenous partial differential equations.

Taking the operator  $\mathbf{D} = -\nabla^2$ ,  $u(\mathbf{x}) = V(x, y, z)$ , and  $f(\mathbf{x}) = \frac{\rho_s(x, y, z)}{\epsilon}$ , equation (A.1) becomes the equation that describes the electric field in the nafion domain.

$$-\nabla^2 V = \frac{\rho_s}{\epsilon} \quad (\text{A.8})$$

By applying the fundamental solution equation, the following becomes the results

$$V(x, y, z) = \frac{1}{\epsilon} \int_{\mathbb{R}^3} G(\mathbf{x}, \boldsymbol{\xi}) \rho_s(\boldsymbol{\xi}) d\boldsymbol{\xi} \quad (\text{A.9})$$

The real struggle is determining the Green's function. By applying this methodology, the Green's function can be determined by solving the following differential equation

$$-\nabla^2 G(\mathbf{x}, \boldsymbol{\xi}) = \delta(x - \xi) \delta(y - \eta) \delta(z - \zeta) \quad (\text{A.10})$$

By applying a 3D Fourier transform with respect to  $x, y$ , and  $z$

$$\tilde{G}(\mathbf{x}, \boldsymbol{\xi}) = \frac{1}{(2\pi)^{3/2}} \int_{\mathbb{R}^3} G(\mathbf{x}, \boldsymbol{\xi}) e^{-i\boldsymbol{\kappa} \cdot \mathbf{x}} d\mathbf{x} \quad (\text{A.11})$$

where  $\boldsymbol{\kappa} = (k, l, m)$ , thus equation (A.9) in the Fourier domain becomes

$$\boldsymbol{\kappa}^2 \tilde{G}(\mathbf{x}, \boldsymbol{\xi}) = \frac{1}{(2\pi)^{3/2}} e^{-i\boldsymbol{\kappa} \cdot \boldsymbol{\xi}} \quad (\text{A.12})$$

now apply the inverse Fourier transform

$$G(\mathbf{x}, \boldsymbol{\xi}) = \frac{1}{(2\pi)^3} \int_{\mathbb{R}^3} \frac{e^{-i\boldsymbol{\kappa} \cdot (\mathbf{x} - \boldsymbol{\xi})}}{\boldsymbol{\kappa}^2} d\boldsymbol{\kappa} \quad (\text{A.13})$$

it should be noted that  $\boldsymbol{\kappa}^2 = \mathbf{k}^T \mathbf{k} = k^2 + l^2 + m^2$

With a change of variables of  $\mathbf{r} = |\mathbf{x} - \boldsymbol{\xi}|$ , the previous equation becomes

$$G(\mathbf{x}, \boldsymbol{\xi}) = \frac{1}{(2\pi)^3} \int_{\mathbb{R}^3} \frac{e^{-i\boldsymbol{\kappa} \cdot \mathbf{r}}}{\boldsymbol{\kappa}^2} d\boldsymbol{\kappa} \quad (\text{A.14})$$

Where this integral can be evaluated in the spherical coordinates, thus with the relationship that  $\boldsymbol{\kappa} \cdot \mathbf{r} = \kappa r \cos(\theta)$  in the spherical coordinates  $(\kappa, \theta, \varphi)$  and  $r = |\mathbf{r}|$ , the previous equation follows as

$$\begin{aligned} G(\mathbf{x}, \boldsymbol{\xi}) &= \frac{1}{(2\pi)^3} \int_{\mathbb{R}^3} \frac{e^{-i\boldsymbol{\kappa} \cdot \mathbf{r}}}{\boldsymbol{\kappa}^2} d\boldsymbol{\kappa} \\ &= \frac{1}{(2\pi)^3} \int_0^\infty \kappa^2 d\kappa \int_0^\pi \sin(\theta) d\theta \int_0^{2\pi} \frac{e^{-i\kappa r \cos(\theta)}}{\kappa^2} d\varphi \\ &= \frac{1}{(2\pi)^2} \int_0^\infty 2 \frac{\sin(\kappa r)}{\kappa r} d\kappa \\ &= \frac{1}{4\pi r} = \frac{1}{4\pi |\mathbf{x} - \boldsymbol{\xi}|} \end{aligned} \quad (\text{A.15})$$

therefore, the fundamental is explicitly

$$V(x, y, z) = \frac{1}{4\pi\epsilon} \int_{\mathbb{R}^3} \frac{\rho_s(\boldsymbol{\xi}, \eta, \zeta)}{|\mathbf{x} - \boldsymbol{\xi}|} d\boldsymbol{\xi} \quad (\text{A.16})$$



Another example could be applying this method to the diffusion equation. An augmented form of the diffusion equation is what governs the cation migration. In order to analytically solve this equation, analysis will be conducted on a simplified version of the diffusion equation. Given that the operator  $\mathbf{D} = \frac{\partial}{\partial t} - D\nabla^2$ ,  $u(\mathbf{x}) = c(x, y, z, t)$ , and  $f(\mathbf{x}) = \Phi(x, y, z)$ , equation (A.1) becomes the equation that describes the diffusion in the nafion domain.

$$\frac{\partial c}{\partial t} - D\nabla^2 c = \Phi(x, y, z, t) \quad (\text{A.17})$$

with boundary conditions that  $t = 0 \Rightarrow c = 0$  and  $c(x, y, z, t) \rightarrow 0$  as  $|\mathbf{x}| \rightarrow \infty, t > 0$

Because we have time in the equation, this has to be taken into account, thus implementation of a joint Laplace and Fourier transform will be used to define the finalized solution. Thus the fundamental solution will be of the form

$$c(x, y, z, t) = \int_0^\infty d\tau \int_{\mathbb{R}^3} G(\mathbf{x}, t; \boldsymbol{\xi}, \tau) \Phi(\boldsymbol{\xi}, \tau) d\boldsymbol{\xi} \quad (\text{A.18})$$

By a similar methodology, the equation for the greens function becomes the following

$$\frac{\partial G}{\partial t} - D\nabla^2 G = \delta(x)\delta(y)\delta(z)\delta(t) \quad (\text{A.19})$$

Here, the joint Laplace and Fourier transform is defined by the following equation

$$\bar{\bar{G}}(\boldsymbol{\kappa}, s) = \frac{1}{(2\pi)^{3/2}} \int_{\mathbb{R}^3} e^{-i\boldsymbol{\kappa} \cdot \mathbf{x}} d\mathbf{x} \int_0^\infty e^{-st} G(\mathbf{x}, t) dt \quad (\text{A.20})$$

Applying this transform to (A.19) produces the following equation

$$\bar{\bar{G}}(\boldsymbol{\kappa}, s) = \frac{1}{(2\pi)^{\frac{3}{2}}} \left( \frac{1}{s + D\boldsymbol{\kappa}^2} \right) \quad (\text{A.20})$$

Where the joint inverse would produce the solution

$$G(\mathbf{x}, t) = \frac{1}{(4\pi Dt)^{\frac{3}{2}}} e^{-\frac{|\mathbf{x}|^2}{4Dt}} \quad (\text{A.20})$$

and if the source was at  $(\xi, \eta, \zeta, \tau)$  rather than  $(0,0,0,0)$ , then the Green's function would become

$$G(\mathbf{x}, t; \xi, \tau) = \frac{1}{(4\pi D(t-\tau))^{\frac{3}{2}}} e^{-\frac{|\mathbf{x}-\xi|^2}{4D(t-\tau)}} \quad (\text{A.21})$$

And the final solution would become

$$c(x, y, z, t) = \int_0^\infty d\tau \int_{\mathbb{R}^3} \left( \frac{\Phi(\xi, \tau)}{(4\pi D(t-\tau))^{\frac{3}{2}}} e^{-\frac{|\mathbf{x}-\xi|^2}{4D(t-\tau)}} \right) d\xi \quad (\text{A.22})$$

## REFERENCES

- [1] D. Pugal, P. Solin, K.J. Kim, and A. Aabloo, “An Explicit Physics-based Model of Ionic Polymer-Metal Composite Actuators,” *Journal of Applied Physics*, Vol. 110, pp. 084904 (2011)
- [2] G. Lee, J. Choi, M. Kim, and S Ahn, “Fabrication and Reliable implementation of an ionic polymer-metal composite (IPMC) biaxial bending actuator”, *Smart Mater. Struct.* 20, pp. 13-26 (2011)
- [3] S. Gutta, J. Realmuto, W. Yim, and K.J. Kim, “ Dynamic Model of a Cylindrical Ionic Polymer-metal Composite Actuator”, *The 8<sup>th</sup> International Conference on Ubiquitous Robots and Ambient Intelligence*, 326-330, (2011)
- [4] W. Yim, J. Renno, and J. Lee, “Dynamic Modeling of Segmented Ionic Polymer Metal Composite(IPMC Actuator”. *International Cont. on Intelligent Robots and Systems*, 326-330, (2011)
- [5] Y. Bar-Cohen(Ed.), “Electroactive Polymer (EAP) Actuators as Artificial Muscles – Reality, Potential and Challenge”, pp. 1-671, SPIE Press, Vol. PM98, (2001)

- [6] Y. Bar-Cohen, X. Bao, S. Sherrit, and S. Lih, "Characterization of the Electromechanical Properties of Ionomeric Polymer-Metal Composite (IPMC)," Proceedings of SPIE's 9<sup>th</sup> Annual International Symposium on Smart Structures and Materials, 17-21 March, 2002, San Diego, CA. Paper No. 4695-27, (2002)
- [7] K. J. Kim and M. Shahinpoor, "A Novel Method of manufacturing Three-Dimensional Ionic Polymer-Metal Composites (IPMCs) Biomimetic Sensors, Actuators and Artificial Muscles," Polymer, vol. 43, no. 3, pp. 797-802, (2002)
- [8] S. Nemat-Nasser and J. Y. Li, "Electromechanical response of ionic polymer-metal composites," Journal of Applied Physics, vol. 87, 3321-3331 (2000).
- [9] M. Shahinpoor and K. J. Kim, "Ionic polymer- metal composites: I. fundamentals," Smart materials and structures, vol. 10, no. 7, 819, (2001)
- [10] T. Wallmersperger, B. J. Akle, D. J. Leo, and B. Kröplin, "Electrochemical response in ionic polymer transducers: An experimental and theoretical study," Composites Science and Technology, vol. 68, no 5, 1173-1180, (2008).
- [11] S. Nemat-Nasser and Y. Wu, "Comparative experimental study of ionic polymer-metal composites with different backbone ionomers and in various cation forms," Journal of Applied Physics, vol 93, no. 9, 5255-5267, (2003).
- [12] D. Pugal, K. J. Kim, M. Kruusmaa, and A. Aabloo, "Finite element simulations of the bending of the ipmc sheet," SPIE, vol. 6524, p. 65240B, (2007).
- [13] M. Shahinpoor, "micro-electro-mechanics of ionic polymeric gels as electrically controllable artificial muscles," Journal of Intelligent Material Systems and Structures, vol 6. No. 3, 307-314, (1995).

- [14] M. Shahinpoor, Y. Bar-Cohen, J. O. Simpson, and J. Smith, "Ionic polymer-metal composites (impccs) as biomimetic sensors, actuators and artificial muscles – a review," *Smart materials and Structures*, vol 7, no. 6, p R15, (1998)
- [15] E. Biddiss and T. Chau, "Electroactive polymeric sensors in hand prostheses: Bending response of an ionic polymer metal composite," *Medical Engineering & Physics*, vol. 28, no. 6, 568-578, (2006)
- [16] S. Lee, H. C. Park, and K. J. Kim, "Equivalent modeling for ionic polymer-metal composite actuators based on beam theories," *Smart Materials and Structures*, 14, 1363–1368, (2005).
- [17] D. Pugal, H. Kasemägi, M. Kruusmaa, and A. Aabloo, "An Advanced Finite Element Model of IPMC" vol. 6927, SPIE 692711-8, (2008)
- [18] K. Newbury, and D. Leo, "Electromechanical modeling and characterization of ionic polymer benders," *Journal of Intelligent Materials Systems and Structures*, 13(1), 51-60, (2002)
- [19] S. Nemat-Nasser, and Y. Jiang, "Electromechanical response of ionic polymer metal composites," *Journal of Applied Physics*, 87(7), 3321-3329, (2000)
- [20] D. J. Segalman, W. R. Witkowski, D. B. Adolf, and M. Shahinpoor, "Theory and application of electrically controlled polymeric gels," *Smart Materials and Structures*, vol.1, no.1, p. 95, 1992
- [21] M. Shahinpoor, "Conceptual design, kinematics and dynamics of swimming robotic structures using ionic polymeric gel muscles," *Smart Materials and Structures*, vol. 1, no. 1, p. 91, 1992

- [22] Parquette, J., Nam, J., and Young, S. “An equivalent circuit model for ionic polymer metal composite and their performance improvement by a clay-based polymer nano composite technique”. *J. Intell. Mater. Syst. Struct.*, 14.
- [23] K, Y., and H, T. “Experimental estimate of viscoelastic properties for ionicpolymer- metal composites”. *Phys. Rev*, 70(052801).
- [24] Mart, A., Alvo, A., Andres, P., and Kruusmaa, M. “A mechanical model of a non-uniform ionomeric polymer- metal composite actuator”. *Smart Mater. Struct*, 17(025004).
- [25] Punning, A., Johanson, U., Anton, M., and Kruusmaa, M. “A distributed model of ipmc”. *Proceedings of SPIE*, 6927.
- [26] Toi, Y., and Kang, S., 2005. “Finite element analysis of two-dimensional electrochemical-mechanical response of conducting polymer-metal composite beams”. *Comput. Struct*, 83, pp. 2573–2583.
- [27] K. M. Newbury and D. J. Leo, “Linear electromechanical model of ionic polymer transducers –part i: Model development,” *Journal of Intelligent Material Systems and Structures*, vol. 14, no. 6, pp.333-342, 2003
- [28] C. Bonomo, L. Fortuna, P. Giannone, S. Graziani, and S. Strazzeri, “A nonlinear model for ionic polymer metal composites as actuators,” *Smart Materials and Structures*, vol. 16, no. 1, p.1, 2007
- [29] R. Caponetto, G. Dongola, L. Fortuna, S. Graziani, and S. Strazzeri, “A fractional model for ipmc actuators,” in *Instrumentation and Measurement Technology Conference Proceedings, 2008. IMTC 2008. IEEE*, pp. 2103-2107, May 2008

- [30] P. Brunetto, L. Fortuna, S. Graziani, and S. Strazzeri, "A model of ionic polymer-metal composite actuators in underwater operations," *Smart Materials and Structures*, vol. 17, no. 2, p. 025029, 2008
- [31] A. J. McDaid, K. C. Aw, E. Haemmerle, and S. Q. Xie, "A conclusive scalable model for the complete actuation response for ipmc transducers," *Smart Materials and Structures*, vol. 19, no. 7, p. 075011, 2010
- [32] M. Kruusmaa, A. Hunt, A. Punning, M. Anton, and A. Aabloo, "A linked manipulator with ion-polymer metal composite (ipmc) joints for soft- and micromanipulation," in *Robotics and Automation, 2008. ICRA 2008. IEEE International Conference on*, pp. 3588-3593, May 2008
- [33] Gennes, P. D., Okumura, K., Shahinpoor, M., and Kim, K., 2000. "Mechanoelectric effects in ionic gels". *EUROPHYSICS LETTERS*, 40, pp. 513–518.
- [34] S. Nemat-Nasser, "Micromechanics of actuation of ionic polymer-metal composites," *Journal of Applied Physics*, vol. 92, no. 5, pp. 2899-2915, 2002
- [35] K. Asaka and K. Oguro, "Bending of polyelectrolyte membrane platinum composite by electric stimuli: Part ii. Response kinetics," *Journal of Electroanalytical Chemistry*, vol. 480, no. 1-2, pp. 186-198, 2000
- [36] M. Porfiri, "Charge dynamics in ionic polymer metal composites," *Journal of Applied Physics*, vol. 104, no. 10, p. 104915, 2008
- [37] Z. Chen and X. Tan, "A control-oriented and physics-based model for ionic polymer-metal composite actuators," *Mechatronics, IEEE/ASME Transaction on*, vol. 13, pp. 519-529, Oct. 2008

- [38] B. J. Akle, W. Habchi, T. Wallmersperger, E. J. Akle, and D. J. Leo, "High surface area electrodes in ionic polymer transducers: Numerical and experimental investigations of the electro-chemical behavior," *Journal of Applied Physics*. Vol. 109, no. 7, p. 074509, 2011
- [39] B. Mead, S. Ruiz, W. Yim, "Closed-loop control of a tube-type cylindrical IPMC", *Proceedings of SPIE Conference, San Diego, CA, 8687-78.*, March 2013
- [40] Logan, D. L. "A first course in the finite element method using algor". PES Publications.
- [41] Gutta, S. K., Trabia, M. B., and Yim, W. "Modeling dynamics of ionic polymer metal composite(ipmc) actuator dynamics using large deflection beam model". *International Mechanical*



## CURRICULUM VITAE

### Siul Ruiz

1460 C Hialeah Dr.  
Las Vegas, NV 89119  
Phone: 702-521-6864  
[Siul.Ruiz@gmail.com](mailto:Siul.Ruiz@gmail.com)

---

#### Summary:

Determined and enthusiastic student seeking engineering experience in an extensive learning environment focusing on dynamical systems, controls, bio-mechanics and finite element modeling

#### Experience:

*June 2012-2013* **Graduate Research Assistant** **University of Nevada, Las Vegas**

- Responsible for developing Finite Element simulations of a cylindrical Ionic Polymer Metal Composite (IPMC) electro active polymer (EAP).
- Responsible for conducting design optimization used to develop specialized IPMC actuators

*June 2009-2012* **Graduate Research Assistant** **Desert Research Institute**

- Responsible for laboratory experiments and Finite Element simulations of the mechanical property of modeling clay in order to gather a quantitative insight on the physical behavior of natural soils.
- Carrying out non-destructive imaging of plant roots in soil at the synchrotron X-ray beam line of the Advanced Light Source, Lawrence Berkeley National Laboratory, Berkeley, Ca. Simulating root-induced deformation of rhizosphere structure based on X-ray CT images using COMSOL Multiphysics
- Presented Poster at the 2010 ASA-CSSA-SSSA International Annual Meeting at Long Beach, CA on Characterizing Mechanical Properties on Modeling Clay.

#### Achievements:

Graduate G.P.A. – 3.85  
 Undergraduate G.P.A. – 3.5  
 Pi-Mu-Epsilon Mathematical Honors society 2009-present  
 Tau-Beta-Pi 2011-Present

**Education:**

2011 – Present M.S. Mechanical Engineering - Dynamics and Controls/Material Mechanics  
 University of Las Vegas, NV  
 2006 – 2011 B.S. Mechanical Engineering - Robotics and Automation  
 University of Las Vegas, NV  
 2006 – 2011 B.S. Mathematical Science - Differential Equations  
 University of Las Vegas, NV

**Activities and Involvement:**

2010 – 2011 Treasurer of the Las Vegas Beta Chapter of the Pi-Mu-Epsilon  
 2009 – 2010 V. Chair of the Student chapter American Society of Mechanical Engineers

**Related Coursework:**

Math431	Differential Equations	ME425	Robotics
Math488	Partial Differential Eqs	ME429	Experimental Vibrations
Math459	Complex Analysis	ME791	LS-Dyna: Dynamic FEA
Math483	General Topology	ME740	Adv. Dynamics
ECG770	Linear Systems Theory	ME747	Biomechanics
Math771	Functional Analysis	ME741	Mechanical Energy Mthds

**Skills:**

Matlab, COMSOL, Hypermesh, LS-Dyna, Solidworks, FORTRAN, C++, UNIX, LABVIEW

**References:**

Available upon request

**Publication List:**

Aravena, J.E., Berli, M., Ruiz, S., Suarez, F., Ghezzehei, T.A., Tyler, S.W., 2013. Quantifying geo-engineering of roots using X-ray microtomography and numerical simulations. Plant and Soil, submitted.

Aravena, J.E., Ruiz, S., Mandava, A.K., Regentova, E.E., Ghezzehei, T.A., Berli, M., Tyler, S.W., 2011. Simulating root-induced rhizosphere deformation and its effect on water flow, American Geophysical Union, Fall Meeting. American Geophysical Union, San Francisco, pp. EOS Abstract No. H51A-1182.

Berli, M., Ruiz, S., Aravena, J.E., Bolduc, L., Ghezzehei, T.A., Cook, D.P., Mandava, A.K., Regentova, E.E., Menon, M., Nico, P.S., Tyler, S.W., Young, M.H., 2011a. Exploring Rhizosphere Structure Alterations Using X-ray Tomography and Finite Element Calculations, DOE Subsurface Biogeochemical Research (SBR) Contractor-Grantee Workshop. US Department of Energy, Office of Science, Washington, DC.

Berli, M., Ruiz, S.A., Aravena, J.E., Bolduc, L., Ghezzehei, T.A., Cook, D.P., Mandava, A.K., Regentova, E.E., Menon, M., Nico, P., Tyler, S.W., Young, M.H., 2011b. Simulating rhizosphere structure alterations using finite element calculations, European Geoscience

- Union General Assembly. European Geoscience Union, Vienna, Austria, pp. EGU2011-13530.
- Keller, T., Lamandé, M., Arvidsson, J., Berli, M., Ruiz, S., Schjønning, P., 2012. Comparing measured with simulated vertical soil stress under vehicle load: are the measurements or the models wrong?, 19th ISTRO Conference. Universidad de la República y el Instituto Nacional de Investigación Agropecuaria, Uruguay, Montevideo, Uruguay, pp. 318-326.
- Ruiz, S., Berli, M., Cook, D.P., 2010. Mechanical characterization of modeling clay, Soil Science Society of America Annual Meeting. Soil Science Society of America, Long Beach, CA.
- Ruiz, S., Berli, M., Cook, D.P., 2013. Mechanical characterization of a visco-elastoplastic clay material: experiments and analytical modeling. Vadose Zone Journal, in preparation.
- Ruiz S., Yun H., Yim W., Kim K., Mead B. (2013) "Design Optimization of Rod Shaped IPMC Actuator", Proceedings of SPIE Conference, San Diego, CA, 8687-54.
- Mead B., Ruiz S., Yim W.(2013) "Closed-loop control of a tube-type cylindrical IPMC", Proceedings of SPIE Conference, San Diego, CA, 8687